

Exploration of potential and free energy surfaces of the neutral Be_4B_8 chiral clusters and their stabilities at finite temperatures.

Carlos Emiliano Buelna-García^{1,2}, César Castillo-Quevedo³, Eduardo Robles-Chaparro⁴, Tristan Parra-Arellano⁴, Jesus Manuel Quiroz-Castillo¹, Teresa del Castillo-Castro¹, Gerardo Martínez-Guajardo⁵, Aned de-Leon-Flores⁴, Gilberto Anzueto-Sánchez⁶, Martha Fabiola Martin-del-Campo-Solis³, Ana Maria Mendoza-Wilson⁷, Alejandro Vasquez-Espinal⁸, and Jose Luis Cabellos^{9**}

¹*Departamento de Investigación en Polímeros y Materiales, Edificio 3G. Universidad de Sonora. Hermosillo, Sonora, México*

²*Organización Científica y Tecnológica del Desierto, Hermosillo 83150, Sonora, Mexico*

³*Departamento de Fundamentos del Conocimiento, Centro Universitario del Norte, Universidad de Guadalajara, Carretera Federal No. 23, Km. 191, C.P. 46200, Colotlán, Jalisco, México*

⁴*Departamento de Ciencias Químico Biológicas, Edificio 5A. Universidad de Sonora. Hermosillo, Sonora, México*

⁵*Unidad Académica de Ciencias Químicas, Área de Ciencias de la Salud, Universidad Autónoma de Zacatecas, Km. 6 carretera Zacatecas-Guadalajara s/n, Ejido La Escondida C. P. 98160, Zacatecas, Zac.*

⁶*Centro de Investigaciones en Óptica, A.C., 37150 León, Guanajuato, México*

⁷*Coordinación de Tecnología de Alimentos de Origen Vegetal, CIAD, A.C., Carretera Gustavo Enrique Astiazarán Rosas, No. 46, Hermosillo 83304, Sonora, México*

⁸*Computational and Theoretical Chemistry Group Departamento de Ciencias Químicas, Facultad de Ciencias Exactas, Universidad Andres Bello, Republica 498, Santiago, Chile*

⁹*Departamento de Investigación en Física, Universidad de Sonora, Blvd. Luis Encinas y Rosales S/N, 83000 Hermosillo, Sonora, México and*

**corresponding author: sollebac@gmail.com, jose.cabellos@unison.mx*

(Dated: July 1, 2021)

Abstract

The lowest-energy structure, distribution of isomers, and their molecular properties depend significantly on the geometry and temperature. The total energy computations under DFT methodology are typically carried out at zero temperature; thereby, entropic contributions to total energy are neglected, even though functional materials work at finite temperature. In the present study, the probability of occurrence of one particular Be_4B_8 isomer at temperature T is estimated within the framework of quantum statistical mechanics and nanothermodynamics. To locate a list of all possible low-energy chiral and achiral structures, an exhaustive and efficient exploration of the potential/free energy surface is done by employing a multilevel multistep global genetic algorithm search coupled to DFT. Moreover, we discuss the energetic ordering of structures computed at the DFT level against single-point energy calculations at the CCSD(T) level of theory. The computed VCD/IR spectrum of each isomer is multiplied by their corresponding Boltzmann weight at temperature T ; then, they are summed together to produce a final Boltzmann weighted spectrum. Additionally, we present chemical bonding analysis using the Adaptive Natural Density Partitioning method in the chiral putative global minimum. The transition state structures and the enantiomer-enantiomer and enantiomer-achiral activation energies as a function of temperature, evidence that a change from an endergonic to an exergonic type of reaction occurs at a temperature of 739 K.

PACS numbers: 61.46.-w,65.40.gd,65.,65.80.-g,67.25.bd,71.15.-m,71.15.Mb,74.20.Pq,74.25.Bt,74.25.Gz,74.25.Kc

Keywords: Global minimum, beryllium-boron cluster, Be_4B_8 , density functional theory, temperature, Boltzmann factors, Gibbs free energy, entropy, enthalpy, nanothermodynamics, thermochemistry, vibrational circular dichroism, IR spectra, quantum statistical mechanics, genetic algorithm, Adaptive Natural Density Partitioning method, DFT, thermodynamics, chiral

I. INTRODUCTION

The potential of boron atom to form stable molecular networks^{1,2} lies in the fact that it has three valence electrons and four available orbitals, which implies it is electron deficient. Moreover, it has a small covalent radius of 0.8-1.01^{3,4} Å, high ionization energy 344.2 kJ/mol,³ and an affinity for oxygen atoms, which is the basis of borates.^{3,5} Boron electron deficiency gives origin to vast number of allotropic forms and uncommon geometries^{2,6,7} such as nanotubes,^{8,9} borospherenes,¹⁰ borophene,⁷ cages,^{9,11} planar,¹² quasi planar,¹³ rings,^{14,15} chiral,^{13,16-20} boron-based helix clusters,^{16,21} and fluxional boron clusters^{2,21-31} that have recently attracted the interest of experimental and theoretical researchers. Since the molecular properties depend greatly on their geometry and temperature;^{32,33} boron cluster exhibit a large number of molecular properties that yield potential applications in medicine,³⁴⁻³⁷ molecular motors,^{21,23,38} superhard materials,³⁹ hydrogen storage,⁴⁰ batteries,⁴¹⁻⁴⁴ catalysis,⁴⁵ and energy materials⁴⁶ among many others.

Particularly, the chirality of nanoclusters has attracted attention due to their chiroptical properties, potential application in efficient chiral discrimination,^{47,48} nonlinear optics⁴⁹ and chiral materials with interesting properties,^{13,50,51} and of course, not to mention that chiral structures play a decisive role in biological activity.⁵²

Previous theoretical studies joint with experimental photoelectron spectroscopy reported the first pure boron chiral B_{30}^- structure as the putative global minimum.¹³ In these pair of planar enantiomers, the chirality arises due to the hexagonal hole and its position. A year later, the lowest energy structures of the B_{39}^- borospherene were reported as chiral due to their hexagonal and pentagonal holes.¹⁷ Similarly, the B_{44} cluster was reported as a chiral structure due to its nonagonal holes.²⁰ That is, in these clusters, holes in the structure cause chirality.

Regarding beryllium-doped boron clusters, they exhibit remarkable properties such as fluxionality,^{7,21,31,53-55} aromaticity,^{21,56} and characteristics similar to borophene.⁵⁷ Furthermore, previous theoretical studies showed that the boron fullerenes B_{60} and B_{80} can be stabilized by surrounding the boron clusters with beryllium atoms,^{58,59} which effectively compensates for boron electronic deficiency.⁵⁹ These effects make beryllium-doped boron clusters interesting.

Particularly attractive are the chiral helices $Be_6B_{11}^-$, reported by Gou et al.²¹, Yanez et

al.,¹⁸ and Garcia-Buelna et al.³³ as one of the low-lying and fluxional isomers, and later a chemical bonding and mechanism of formation study of the beryllium-doped boron chiral cluster $\text{Be}_6\text{B}_{10}^{2-}$ and coaxial triple-layered $\text{Be}_6\text{B}_{11}^-$ sandwich structure were reported.^{16,55} In these structures, the chirality arises due to the formation of a boron helix.

However, there are only a few theoretical studies on vibrational circular dichroism (VCD) and infrared spectroscopy (IR) as a function of temperature in beryllium-boron clusters^{33,60}. We emphasize that there are neither theoretical nor experimental studies of VCD / IR spectra in chiral Be_4B_8 clusters, although VCD/IR spectra give insight into the geometrical structure.⁶¹⁻⁶⁴ Recently, Castiglioni et al. reviewed experimental aspects of solid-state circular dichroism,⁶⁵ and Avilés Moreno et al. reported the experimental and theoretical IR/VCD spectra of various compounds.⁶⁶⁻⁶⁹ VCD is differential spectroscopy sensitive to the difference in the absorption for the left and right polarized light.^{61,64,70} It usually is four times in magnitude smaller than IR absorption⁷¹ and yields information on the lowest energy conformation in solution;⁷² thus, the chiral molecule's absolute configuration can be determined employing the VCD spectra.⁷³

The IR frequencies are related to the second derivative of the potential energy and they are useful in identifying transition states and computing thermodynamics through the vibrational partition function.^{33,74,75} Additionally, the structure of neutral boron clusters B_{11} , B_{16} and B_{17} was probed by IR.⁷⁶

The DFT VCD/IR spectra depend on the functional and basis set employed⁶³ and significantly on the lowest- and the low-energy achiral and chiral structures, so we need an efficiently sampling of the free energy surface to know the distribution of isomers at different temperatures.^{32,33,77-80} A considerable change in the isomer distribution and the energetic separation among them is the first notable effect of temperature.^{33,77} Useful materials work at finite temperatures; in that conditions, Gibbs free energy is minimized⁸¹ and determines the putative global minimum at given temperature,³³ whereas, entropy of the atomic cluster is maximized.⁸¹ Although in the mid 1960's, Mermin et al.⁸² studied the thermal properties of the inhomogeneous electron gas, most of DFT calculations are typically performed at zero temperature. Recently, over again, DFT was extended to finite temperature,⁸³⁻⁸⁵ but nowadays, as far as we know, it is not implemented in any software. However, molecular dynamics and other simulation tools have been employed to study atomic clusters at finite temperatures.^{27,29,86-89}

In this study, based on the Gibbs free energy of each isomer and Boltzmann factors, we computed the probability of occurrence (Boltzmann weights) of each particular isomer of Be_4B_8 as a function of temperature using quantum statistical mechanics. The computed VCD/IR spectrum of each isomer is multiplied by their corresponding Boltzmann weight at temperature T ; then, they are summed together to produce a final Boltzmann weighted spectrum. In the mid 1980, P. J. Stephens with co-workers implemented the atomic axial tensors in Gaussian 80 code that allows them to compute the VCD spectrum of propylene oxide and compare with the experimental spectrum⁹⁰ Later, Nafie and Stephens employed the Boltzmann weights scheme, they computed the VCD spectrum for each isomer, and the total resulting spectra were averaged and weighted by Boltzmann factors.^{61,91-93} Recently these factors were used in other previous works.^{33,78-80,83,94}

To achieve the mentioned above, we located all low-energy structures on the potential and free energy surfaces of the Be_4B_8 cluster with a genetic algorithm coupled to DFT and computed the Boltzmann weights in temperatures ranging from 20 to 1900 K. We also located the solid-solid transformation point at 739 K, where chiral and achiral structures coexist, and computed the energy barrier (E_a) for temperatures ranging from 20 to 1900 K for transformation of enantiomers (plus, \mathcal{P}) to an achiral structure. We locate the T_{ee} point is defined here as the temperature where the reaction change from endergonic to exergonic. Moreover, the energy of enantiomerization was computed between \mathcal{P} and minus (\mathcal{M}) enantiomers, and we defined the T_{bb} point in scale temperature where the energy barrier of two possible reaction mechanisms is equal to each other, which implies the velocity of the reaction is equal for both mechanisms. We investigated how the symmetry point group affects the Gibbs free energy. Our results show that the chirality on Be_4B_8 arises from the Be-Be dimers capping the boron ring and also of the distorted boron ring, thus, the lowest energy chiral structure is favored by the interaction between beryllium and the boron framework. The high energy of enantiomerization of the Be_4B_8 cluster in temperatures ranging from 20 to 1900 K suggests that it is a good candidate for applications; only one of the enantiomers shows the desired effect. The computed enthalpy of formation (ΔH) between chiral and achiral structure at 739 K show that there is a change from endo to exothermic reaction. Our results indicate that the Boltzmann weighted VCD spectrum is zero in all range of temperature, whereas, the Boltzmann IR weighted spectrum is strongly dominated by the lowest energy pair of enantiomers. the remainder of the manuscript is

organized as follows: Section 2 gives the computational details and a brief overview of the theory and the algorithms used. The results and discussion are presented in section 3. We discuss the effect of the symmetry in the energetic ordering and clarify the origin of the 0.41 kcal/mol difference energy between two structures with symmetries C_2 and C_1 that appear when we compute the Gibbs free energy. A comparison among energies computed at a single point CCSDT against DFT levels of theory and the \mathcal{T}_1 diagnostic is presented. We do the chemical bonding analysis by employing the AdNDP scheme to \mathcal{P} minimum energy structure. The interconversion energy barrier between the \mathcal{P} and \mathcal{M} enantiomers and between an achiral structure and \mathcal{P} enantiomer are discussed in terms of temperature. IR spectra are analyzed as a function of temperature. Conclusions are given in Section 4.

II. THEORETICAL METHODS

A. Global Minimum Search and Computational Details

First of all, for theoretical studies of an atomic cluster, the first step is locating the putative global minimum and all the closet low-energy structures on its potential/free energy surface, since the measured molecular properties are statistical averages over the ensemble of conformations.^{33,95} We must keep in mind that experimental atomic molecular studies are conducted in non-zero temperatures while theoretical studies based on density functional theory computations are performed at zero temperature.⁹⁶ If the temperature increases, Gibbs free energy determines the lowest-energy structure,³³ and the entropy of the atomic cluster is maximized,⁸¹ while at temperature zero, the enthalpy determines the putative global minimum. Secondly, the search of the global minimum in atomic clusters is a complicated task due to the degrees of liberty increase as a function of the number of atoms. Consequently, the number of possible combinations grows exponentially, leading to a combinatorial explosion problem.⁹⁷ Thirdly, a systematic and exhaustive exploration of the multidimensional potential/free energy surface, avoiding an incomplete sampling of the configuration space is needed.^{33,78,79} Finally, it is important to take into account all low-energy structures with all low-symmetries due to the influence of the point group symmetry of the molecule on the Gibbs free energy through rotational entropy, which is a function of the symmetry number that appears in the rotational entropy denominator. This could affect the relative popula-

tions leading to miscalculation of molecular properties when they are computed employing weighted Boltzmann factors.³³ Despite the difficulties mentioned above, several algorithms to explore the potential/free energy surface coupled to an any electronic structure package have been successfully employed so far, such as *AIRSS* approach,⁹⁸ simulated annealing,^{99–104} kick methodology^{105–117} and genetic algorithms^{9,21,33,112,116,118–123} among others. Our computational procedure to explore the potential/free energy surface of the neutral Be_4B_8 cluster employs a hybrid genetic algorithm implemented in *GALGOSON* code.^{33,77} This methodology based on previous works^{21,116,124,125} consists of a multi-step approach (cascade) to efficiently sample the potential/free energy surface coupled to the *Gaussian*¹²⁶ code. Our multi-step strategy employs more accurate levels of theory applied to each step to arrive at the most stable lowest-lying isomers. In the first step of our methodology, the code builds an initial random population of planar and 3D structures (two hundred structures per atom of the Be_4B_8 cluster) employing a strategy used in previous work.^{21,33,113,116,118,121,125,127} Then, structures are optimized at the PBE0¹²⁸/LANL2DZ¹²⁹ level of theory with Gaussian 09 code. Here we consider that the overall global search methodology might be sped up using a smaller basis set, in early stage. The PBE0 functional has shown good performance in pure and doped boron clusters,^{18,21,33,130,131} moreover, energetic analysis of anionic Be_6B_{11} cluster in several previous works were done employing PBE0 functional^{18,21,33} Additionally, relative energies at the PBE0 level are similar to those the CCSD(T) level in B_9^- boron cluster.¹³² As a second step, with the aim of increasing the performance, and deciding if a structure should be further relaxed; *GALGOSON* makes a cluster shape comparison among them by a superposition method¹³³; All isomers that lie below $20 \text{ kcal}\cdot\text{mol}^{-1}$ on the energy scale are permitted to relax, and they compose the first cluster population of the genetic algorithm. The optimization in this step is done at the PBE0¹²⁸/def2TZVP^{134,135} level of theory, including Grimme’s dispersion (GD3) effects¹³⁶ as implemented in Gaussian 09 code. The criterion to stop the algorithm is that the lowest energy structure persists for five generations. In the third step, structures lying within $20 \text{ kcal}\cdot\text{mol}^{-1}$ found in the previous step are symmetrized at the low-symmetry point group. Those structures are the initial population for the genetic algorithm at the PBE0-GD3/def2-TZVP level, taking into account the zero-point energy (ZPE) corrections. In total at this point and in all previous stages, about 2800 relaxations to a local-energy minimum were performed. Additionally, we make sure that the lowest vibrational mode of each isomer is positive to identify a valid energy mini-

mum and discard transition states. In the final step, single point (SP) computations for the low-energy structures lying below 8 kcal·mol⁻¹ carried out at CCSD(T)/def2-TZVP//PBE0-D3/def2-TZVP level of theory as it is implemented in Gaussian 09 code.¹²⁶ Moreover, SP were computed employing the domain-based local pair natural orbital coupled-cluster theory (DLPNO-CCSD(T)), with and without taking into account the ZPE correction energy. Furthermore, to determine if the energy evaluation scheme based on a single reference method of the Be₄B₈ cluster, contains a substantial multireference character. We computed the \mathcal{T}_1 diagnostic. Our results confirm that the computed \mathcal{T}_1 diagnostic values are below the recommended threshold of 0.02^{125,137} for all low-energy isomers and ensure that DFT energies of Be₄B₈ do not contain a large multireference character. Hernandez et al.¹²⁵ found similar values for \mathcal{T}_1 descriptor in doped Boron clusters. The \mathcal{T}_1 diagnostic and the SP calculations at DLPNO-CCSD(T) level were performed using ORCA program suite,¹³⁸ with *TightPNO* settings.¹³⁹ Chemical bonding was examined using the Adaptive Natural Density Partitioning (AdNDP) method.¹⁴⁰ AdNDP analyses the first-order reduced density matrix and recovers Lewis bonding (1c-2e or 2c-2 e, i.e., lone pairs or two-center two-electron bonds) and delocalized bonding elements associated with the concept of electron delocalization.

B. Thermochemistry Properties

The molecular partition function contains all thermodynamic information in a similar way that the wavefunction contains all the information about the system.^{33,74} which implies that all thermodynamic properties of an ensemble of molecules can be derived from this function. Previous theoretical studies used the partition function to compute temperature-dependent entropic contributions¹⁴¹ on [Fe(pmea)(NCS)₂] complex, infrared spectroscopy on anionic Be₆B₁₁ cluster,³³ and rate constant.⁷⁴ In this study, the thermodynamic functions dependent on temperature are computed employing the partition function Q shown in Equation 1, and computed under the rigid rotor, harmonic oscillator, Born-Oppenheimer, ideal gas, and a particle-in-a-box approximations.

$$Q(T) = \sum_i g_i e^{-\Delta E_i / k_B T} \quad (1)$$

In Eq. 1, g_i is the degeneracy factor, k_B is the Boltzmann constant, T is the temperature, and $-\Delta E_i$ is the total energy of a cluster.^{33,74,142} We employ equations 2 to 5 to compute the

internal energy (U), enthalpy (H), and Gibbs energy (G) of the Be₄B₈ cluster at temperature T. The equations 1 to 4 and the equations to compute entropy contributions (S) are those employed in a previous work^{33,74,77} and any standard thermodynamics textbook.^{142,143}

$$\mathcal{U}_0 = \mathcal{E}_0 + ZPE \tag{2}$$

$$U_T = \mathcal{U}_0 + (E_{ROT} + E_{TRANS} + E_{vib} + E_{elect}) \tag{3}$$

$$H = U_T + RT \tag{4}$$

$$G = H - TS \tag{5}$$

In Equations above, ZPE is the zero-point energy correction \mathcal{E}_0 is the electronic energy, and $E_{ROT} + E_{TRANS} + E_{VIB}$ are the contributions to energy due to translation, rotation, and vibration as function of temperature, respectively. In order to compute the probability of occurrence of one particular cluster in an ensemble of Be₄B₈ clusters (Boltzmann ensemble at thermal equilibrium) as a function of temperature, we employ the probability of occurrence^{33,74,79,80,144–149} given in Equation 6

$$P_i(T) = \frac{e^{-\beta\Delta G^k}}{\sum e^{-\beta\Delta G^k}}, \tag{6}$$

where $\beta = 1/k_B T$, and k_B is the Boltzmann constant, T is the temperature, and ΔG^k is the Gibbs free energy of the k^{th} isomer, Any molecular properties observed are statistical averages over a Boltzmann ensemble of clusters, then for an ensemble of clusters, any property can be computed as an average of all possible conformations.^{33,147} Equation 6 is restricted so that the sum of all probabilities of occurrence, at fixed temperature T, $P_i(T)$ must be equal to 1 given, according to Equation 7

$$\sum_i P_i(T) = 1, \tag{7}$$

In this study, the Boltzmann weighted VCD/IR spectrum (VCD/IR_{Bolt}) at temperature T is given by Equation 8

$$VCD/IR_{Bolt} = \sum_i^n VCD_i/IR_i \times P_i(T) \tag{8}$$

Where n is the total number of cluster in the ensemble, VCD/IR_{*i*} is the VCD/IR of the i^{th} isomer at temperature T=0, and $P_i(T)$ is the probability of the i isomer given by Equation 6.

The sum only runs over all achiral, Plus and Minus isomers. For achiral structures the VCD is equal to zero and there is no contribution to VCD_{Bolt} . Here, we point out that is important to take into account the achiral structures due to the probability of a particular chiral cluster changing as consequence of the VCD_{Bolt} . in spite of the VCD for achiral structures being zero. For the computation of relative populations and VCD/IR_{Bolt} spectra, we used the Boltzmann-Optics-Full-Ader code (*BOFA*) that is part of spectroscopy capabilities of *GALGOSON* code.³³

III. RESULTS AND DISCUSSION

A. The lowest energy structures and energetics

Figure 1 shows the low-energy configurations of Be₄B₈ clusters optimized at PBE0-GD3/def2-TZVP level of theory taking into account ZPE energy correction. The optimized average B-B bond length of the putative chiral global minimum is 1.5867 Å, in good agreement with an experimental bond length of 1.57-1.59 Å.^{150,151} and also within agreement with others previous DFT calculations.³³ The most recurring motif within the lower energy isomers of B₈Be₄ is a sandwich structure,(SSh) in which the boron atoms form a hollow distorted ellipsoid ring with each of the Be-Be dimers capping the top and bottom with C₁ point group symmetry. Isomers *a* and *b* and also listed as *i*₁ and *i*₂ in Table I, are enantiomers differing in the orientation of the Be-Be dimers with respect the boron skeleton. Based on the B-B bond length evolution along the intrinsic reaction coordinate (IRC) (See movie in Supporting Material) between Plus-enantiomer-Minus-enantiomers, and displayed in Figure 10 appendix B the shortest B-B bond length is located at the transition state structure. In contrast, the largest B-B bond length is located in the reactant and product points. On the other hand, appendix Figure 10 appendix B shows the distance evolution between (Be-Be)-(Be-Be) dimers; one can see the largest distance between dimers is located at the transition state, whereas the shortest distance is located at the product and reactants points. From the above mentioned, the B-B interaction does not favor the formation of the lowest energy enantiomers structures; meanwhile, the Be-Be interaction promotes the lowest energy structure to be chiral. Here, we infer that the Be-B interaction also favors the chiral lowest energy structures. The Be-Be bond length for the six lowest energy enan-

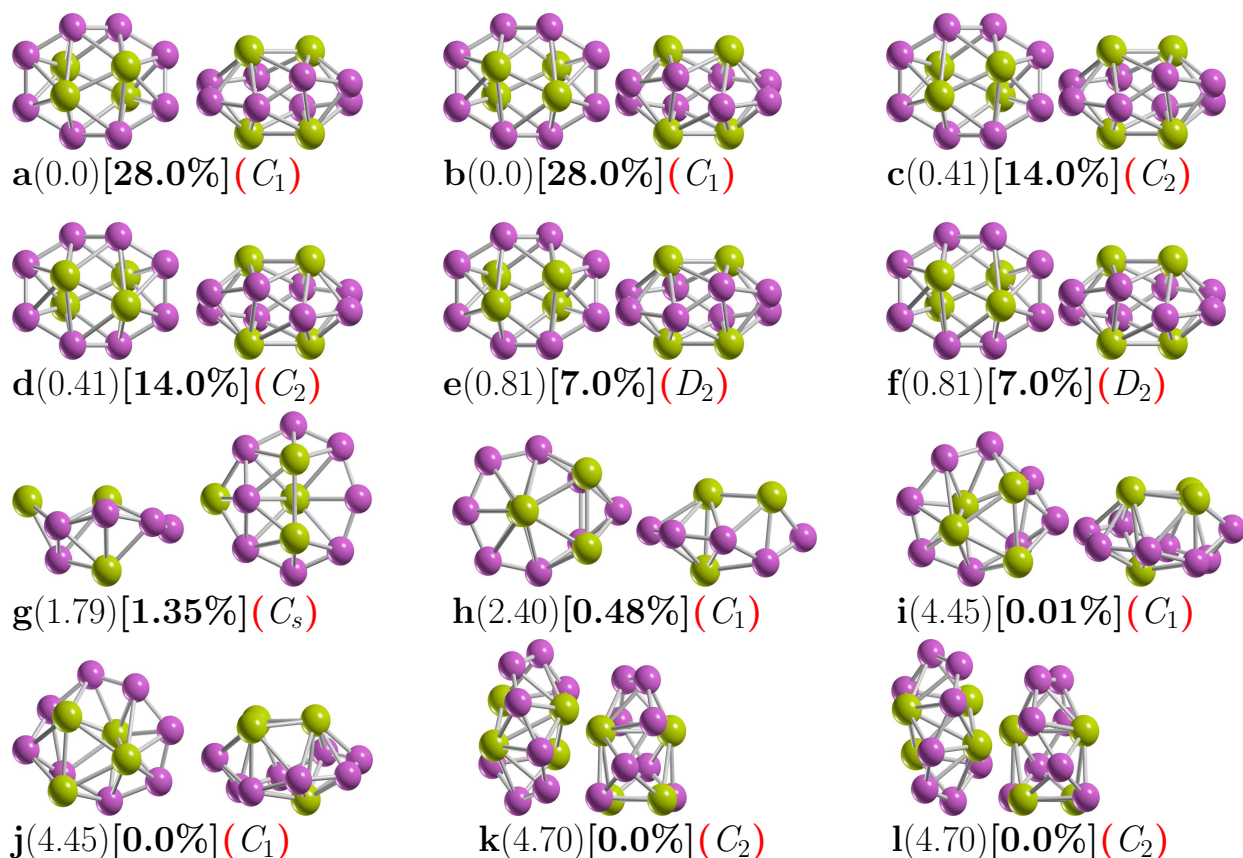


FIG. 1: (Color online) Optimized geometries of neutral Be_4B_8 cluster at PBE0-GD3/def2TZVP level of theory with ZPE correction energy. They are shown in two orientations, front, and rotated 90 degrees up to paper plane. The lower-case letter is the isomer label, relative Gibbs free energies in kcal/mol (in round parenthesis) at 298.15 K, the relative population [in square parenthesis], and group symmetry point (in red round parenthesis). The structures with label (a,b), (c,d), (e,f), (i,j) and (k,l) are chiral. The purple- and yellow-colored spheres represent the boron and beryllium atoms, respectively.³³ Atomic Cartesian coordinates of these isomers are provided in Supporting Material.

The bond lengths of the Be-Be in the isomers is 1.9874, 1.9876, and 1.9881 Å for symmetries C_1 , C_2 , and D_2 , respectively, in good agreement with the bond length of the Be-Be in Be_2B_8 cluster 1.910 Å.⁵³ To gain more insight into the chemical bonding, an AdNDP analysis of the lowest energy isomer was performed (Figure 2). The AdNDP analysis for this chiral structure revealed the presence of eight 2c-2e B-B σ -bonds with an occupation number (ON) between 1.92 and 1.94 —e— and three delocalized σ -bonds throughout the B_8 ring with an ON between 1.95 and 1.99

—e—. Additionally, three distorted π -bonds (due to the non-planarity of the structure), one of which is delocalized over all eight boron atoms and the other two involving four boron and two beryllium atoms (one from the top and one from the bottom). Finally, the bonding pattern is completed by two 6c-2e σ -bonds with main contribution coming from the interaction between the two Be atoms from the top and bottom, respectively. The isomers with

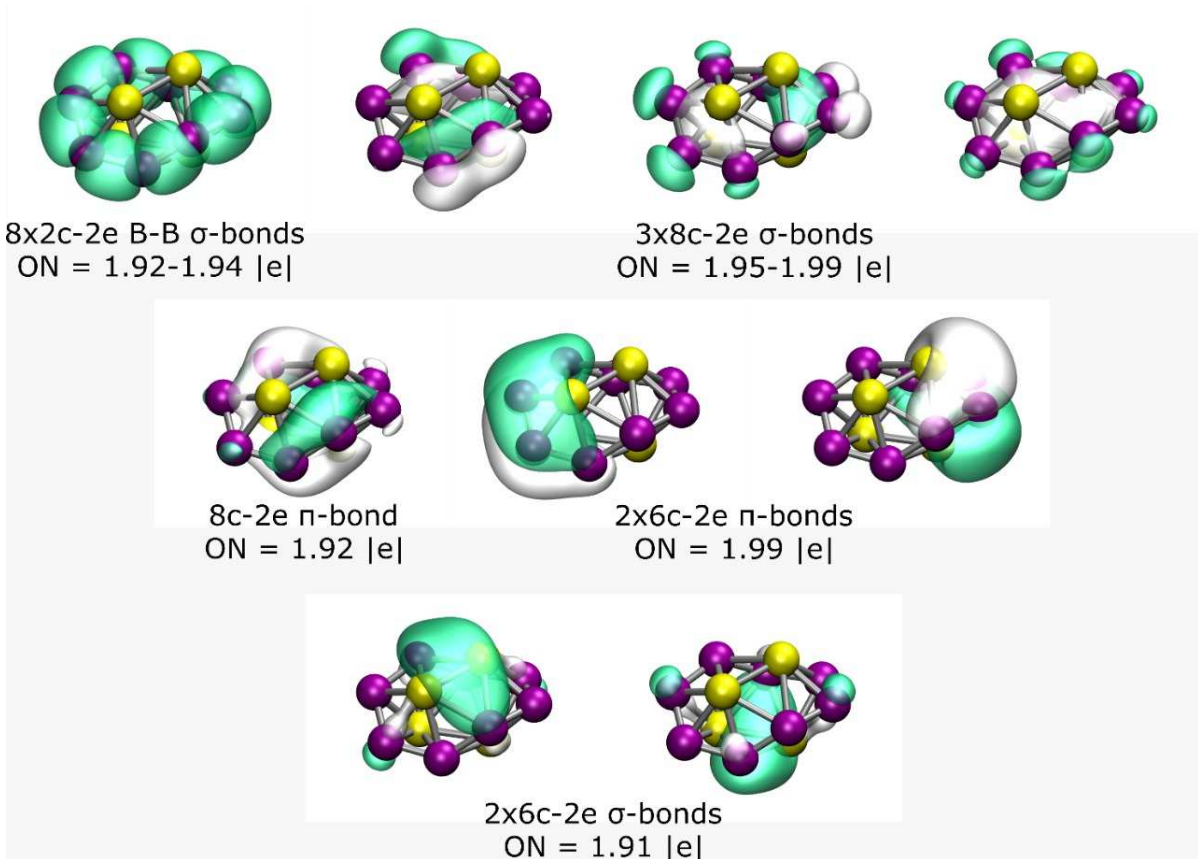


FIG. 2: (Color online) Results of the AdNDP analysis of the lowest-energy chiral isomer of the Be_4B_8 system.

symmetry C_1 are the most energetically favorable, with 28% each of the Boltzmann population at 298.15 K. An exhaustive and systematic exploration of the potential energy surface considering triplet states revealed that the lowest triplet ground state lays 13.7 kcal/mol above the singlet putative chiral global minimum single ground state, which is too far away energetically to be considered. Next, low-energy SSh-isomers labeled i_3 and i_4 in Table I, and depicted in Figure 1(3,4) lies just 0.41 kcal/mol above the putative global minimum, it is a similar-SSh structure than the putative global minimum, only with C_2 point group

symmetry, followed by slightly higher energy and similar-SSh structure located just 0.81 kcal/mol above the putative minimal structure with D_2 point group symmetry. We point out that the unique differences among these chiral structures are the different symmetry point groups. The most energetically favorable is the non symmetry (C_1) cluster; moreover, these six structures contribute to 98% to the relative population at 298.15 K. The next

TABLE I: Single point relative energy calculations of the low-energy structures at different levels of theory. Coupled Cluster Single-Double and perturbative Triple, (CCSD(T)), CCSD(T) with zero point energy (\mathcal{E}_{ZPE}), (CCSDT+ \mathcal{E}_{ZPE}), CCSD(T) employing the domain-based local pair natural orbital coupled-cluster theory (DLPNO-CCSD(T)), with TightPNO setting, with zero point energy (DLPNO-CCSD(T)+ \mathcal{E}_{ZPE}), Gibbs free energy (ΔG) at 298.15 K, Electronic energy with ZPE ($\mathcal{E}_0 + \mathcal{E}_{\text{ZPE}}$), Electronic energy (\mathcal{E}_0), point group symmetry, and \mathcal{T}_1 Diagnostic. All relative energies are given in kcal·mol⁻¹

Level	Isomers									
	i_1	i_2	i_3	i_4	i_5	i_6	i_7	i_8	i_9	i_{10}
ΔG	0.0	0.0	0.41	0.41	0.81	0.81	1.79	2.40	4.45	4.45
CCSDT	0.0	0.0	0.0	0.0	0.0	0.0	3.61	3.38	5.38	5.38
CCSDT+ \mathcal{E}_{ZPE}	0.0	0.0	0.0	0.0	0.0	0.0	2.71	2.51	4.51	4.51
DLPNO-CCSD(T)	0.0	0.0	0.0	0.0	0.0	0.0	0.75	1.37	5.0	5.0
DLPNO-CCSD(T)+ \mathcal{E}_{ZPE}	0.0	0.0	0.0	0.0	0.0	0.0	-0.20	0.50	4.10	4.10
$\mathcal{E}_0 + \mathcal{E}_{\text{ZPE}}$	0.0	0.0	0.0	0.0	0.0	0.0	2.38	2.80	5.03	5.03
\mathcal{E}_0	0.0	0.0	0.0	0.0	0.0	0.0	3.28	3.68	5.90	3.28
Point group symmetry	C_1	C_1	C_2	C_2	D_2	D_2	C_s	C_1	C_1	C_1
\mathcal{T}_1 Diagnostic	0.019	0.019	0.019	0.019	0.019	0.019	0.016	0.015	0.016	0.016

higher energy structure, labeled as i_7 in Table I and depicted in Figure 1(g), is located at 1.79 kcal/mol above the putative minimum global at 298.15 K, with symmetry C_s . It is also a sandwich structure formed by a distorted circular ring in which one of the Be-Be dimers is capping in the center of the ring, and the other one is located on one face of the

boron circular ring. This structure is achiral, and its probability of occurrence is 1.35% at 298.15 K. Next achiral isomer lies 2.40 kcal/mol above the putative minimum global with C_1 symmetry, labeled as i_8 in Table I and depicted in Figure 1(8). It is also a sandwich-type structure formed by a distorted circular boron ring with three boron atoms capping one side of the ring and the other Be atom capping the other. The probability of occurrence of this isomer at 298.15 K is just 0.48% and its contribution to chiroptical spectroscopies is negligible. The next two chiral structures lies 4.45 kcal/mol above the putative global minimum with C_1 symmetries, labeled as i_9 and i_{10} in Table I and depicted in Figure 1(i,j). They are sandwich-type structures formed by a non-planar distorted circular boron ring with three Be atoms capping one side of the boron ring and the other Be atom is located on the other face, and in the center of the distorted boron ring; Its Boltzmann probability of occurrence is zero at 298.15 K, so as a consequence, at this temperature, its contributions to any chiroptical spectroscopies are negligible. The following chiral higher energy structure, with C_2 point group symmetry, lies 4.70 kcal/mol energy above the putative global minimum. It is a chiral helix type structure depicted in Figure 1(12,13); it has four Be atoms located in the center of the boron spiral, this helix structure is similar to those found by previous theoretical works^{18,21,33} and its probability of occurrence is negligible at room temperature. To gain insight into the energy hierarchy of isomers and validate our DFT calculations, relative energies were computed at different levels of theory, and differences between them are shown in Table I. Energy computed at different methods yield different energies due mainly to the functional and basis-set employed,^{33,152} so the energetic ordering change; consequently, the probability of occurrence and the molecular properties will change. The first line of Table I shows the relative Gibbs free energy computed at PBE0-GD3/def2-TZVP and room temperature. The small relative Gibbs free energies (0.41, and 0.81 kcal/mol) differences among the six enantiomer structures i_1 to i_6 in Table I are caused by the rotational entropy being a function of the symmetry number that in turn depends on the point group symmetry. An increase/decrease in the value of rotational entropy changes the Gibbs free energy. The Gibbs free energy computed with and without symmetry will differ by a factor $RT\ln(\sigma)$. Here, R is the universal gas constant, T, the temperature, and σ is the symmetry number. Figure 3 shows the factor $RT\ln(\sigma)$ for temperatures ranging from 0 to 1900 K and for different symmetry number values ($\sigma=2,3,4,5$). A closer analysis of Figure 3, shows that at room temperature $RT\ln(\sigma)=0.41$ kcal/mol with $\sigma=2$, and $RT\ln(\sigma)=0.81$ kcal/mol with $\sigma=4$, in

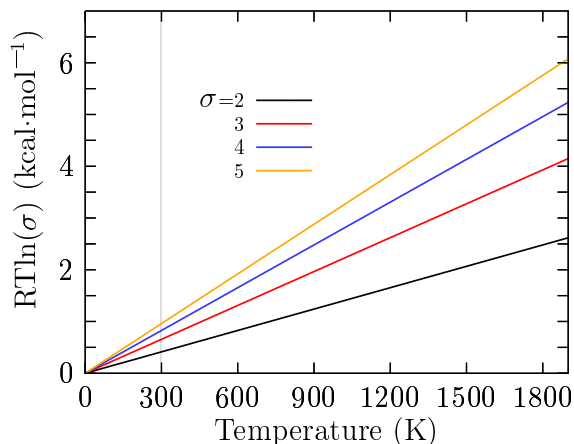


FIG. 3: (Color online) The difference of the rotational entropy computed with and without symmetries is given by a factor of $RT\ln(\sigma)$ in kcal/mol; in this factor, R is the universal gas constant, T , the temperature, and σ is the symmetry number (The factor is similar to the enantioselectivity¹⁵³). These values, at 298.15 K, are in good agreement with the values shown in the first line of Table I (0.41 and 0.81 kcal/mol).

agreement with the values shown in the first line of Table I. As the temperature increases, the energy differences between the factors $RT\ln(\sigma)$ become larger. These small relative Gibbs free energies are responsible for different values of probability of occurrence at low temperatures for the similar isomers with different point group symmetry. This strongly suggests that there must be atomic clusters with low and high symmetries in the Boltzmann ensemble to compute the molecular properties correctly. The second line in Table I shows single point (SP) relative energies computed at the CCSD(T)¹⁵⁴, the energetic ordering of isomers listed in the first line of Table I follows almost the trend of energetic ordering at SP CCSD(T) level, notice that just the achiral isomers label i_7 to i_8 in Table I are interchanged in energetic ordering. The third line Table I shows single point relative energies computed at the CCSD(T)¹⁵⁴/def2-TZVP//PBE0-GD3/def2-TZVP; the energetic ordering is similar to pure CCSD(T) energy. DLPNO-CCSD(T) relative energies, with and without ZPE correction, are shown in lines four and five of Table I, the first follows the trend of pure CCSD(T) energy, and the second, the ZPE value, interchange the isomers, label i_7 in Table I, to be the putative global minimum. Here we can say that the ZPE energy inclusion is essential in distributing isomers and molecular properties. The sixth and seventh lines of Table I show

the electronic energy with and without ZPE correction, and both of them follow the trend of the Gibbs free energy given in line number one. Line number 8 in Table I shows the point group symmetry for each isomer. The T_1 diagnostic for each isomer is shown inline nine of Table I, all of them are lower than the recommended value 0.02^{125,154} so the systems are appropriately characterized.

B. Structures and Stability at Finite Temperature.

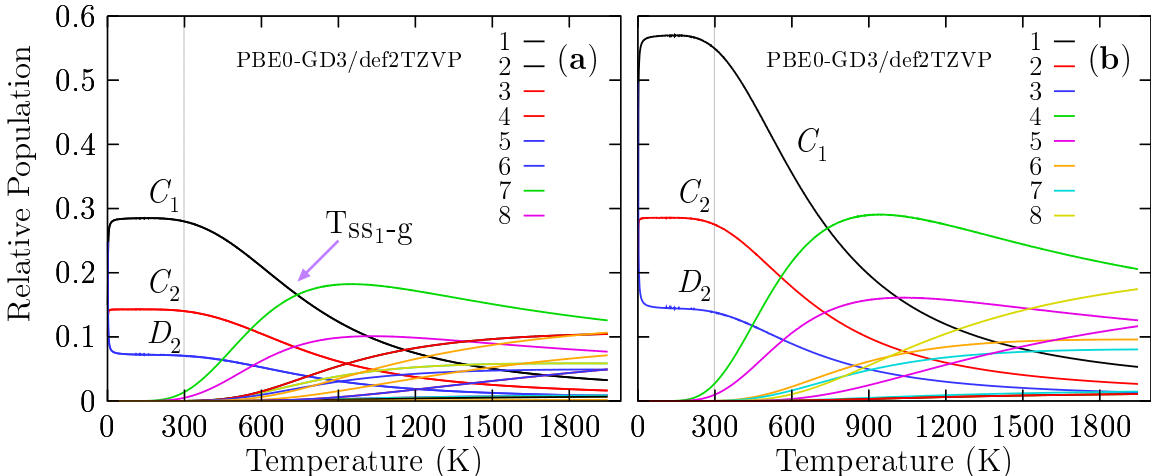


FIG. 4: (Color online) The left panel (a) shows the probability of occurrence for temperatures ranging from 20 to 1900 K at the PBE0-GD3/def2-TZVP level of theory considering that the Boltzmann ensemble is composed of achiral structures and an equal mixture of \mathcal{P} , and \mathcal{M} enantiomers which implies, a Boltzmann racemic ensemble. The right panel (b) shows the probability of occurrence for temperatures ranging from 20 to 1900 K at the PBE0-GD3/def2-TZVP level of theory taking into account only the achiral structures and \mathcal{M} enantiomers, which implies Boltzmann pure ensemble of only one enantiomer. percent enantiomeric excess is 100%. (Boltzmann pure ensemble of only one enantiomer) In panel (a) the transition solid-solid point (T_{ss1-g}) is located at 739 K with 16.6% of probability, while in panel (b) the T_{ss1-g} is located at 739 K with 27% probability. The lowest-symmetry C_1 is strongly dominating at temperatures from 20 to 739 K due to rotational entropy that is a function of the point group symmetry.

As we mentioned earlier, the determination of the structure is the first step to study any property of a material. Moreover, we have to consider that an observed molecular

property in a Boltzmann ensemble is a weighted sum of all individual contributions of each isomer that form the ensemble. At temperature 0 K, the electronic energy plus zero-point energy determine the putative global minimum and all nearby low-energy structures (PGMLES), whereas, at temperatures larger than 0 K, the Gibbs free energy defines the PGMLES. Figure 4 shows the probability of occurrence for each particular chiral and achiral Be_4B_8 isomers for temperatures ranging from 20 to 1900 K. In panel (a) the probability of occurrence is shown, taking into account the \mathcal{M} , \mathcal{P} , and achiral structures, which implies Boltzmann racemic ensemble (the percent enantiomeric excess is zero (Boltzmann racemic ensemble). whereas panel (b) shows the probability of occurrence only taking into account just the \mathcal{M} handled and achiral structures, which implies that the percent enantiomeric excess is 100%. then the ensemble is a Boltzmann pure ensemble of only one type of enantiomer. There is a significant difference in the probability of occurrence between the two panels. In panel (a), we consider the \mathcal{P} and \mathcal{M} structures, and both structures possess the same probability of occurrence in all ranges of temperature. All the probabilities of occurrence (chiral) shown in panel (b) are approximately two times the probability of occurrence (chiral) shown in panel (a). A closer examination of the panel (a) shown that in the temperature ranging from 20 to 300 K, all molecular properties are dominated by chiral structure depicted in Figure 1(a,b) because its probability of occurrence is almost constant. We point out that in this range of temperature, the C_1 , C_2 and D_2 symmetries strongly dominate with different probabilities of occurrence of 28, 14 y 7% respectively. This different probability of occurrence for the same structure with only different symmetries is due to rotational entropy, that also is responsible for those slight energy differences shown in Table I and, in turn, it is the reason for the differences in the probability. At temperatures above 300 K, the probability of occurrence of the putative global minimum at cold temperatures and depicted in solid-black line decay exponentially up to 1900 K. The dominant transformation solid-solid point ($T_{\text{ss1-g}}$) is located at 739 K with 16.6% of probability. At this point, there is a co-existence of chiral structures and achiral structures, shown in Figure 1(a,g), above this point the achiral structure (Figure 1(g)) become dominant. Its probability of occurrence is depicted in the solid-green line in Figure 4a and start to grow up at almost at room temperature. The second transformation solid-solid point located at 1017 K and 10% of probability also coexist the chiral putative global minimum with symmetry C_1 and achiral structure (Figure 1(h)) located at 2.40 kcal/mol Gibbs free energy at 298.15 K above the putative global

minimum. Figure 4b shows the computed probability of occurrence considering the percent enantiomeric excess is one hundred percentage, which implies of a pure Boltzmann ensemble of only one type of enantiomer. With the aim to compute the Boltzmann VCD/IR weighted spectra as a function of temperature, we take the relative population shown in Figure 4a. The probability of the dominant achiral putative global minimum with symmetry C_1 is depicted in the solid-green line in Figure 4a. Analysis of the probability of occurrence leads to an interesting observation: The individual putative minimum global strongly dominates the VCD/IR at a temperature ranging from 20 to 1240 K. The achiral structures have a zero contribution to VCD in hot temperatures. The probability of occurrence is dependent on the functional and basis set employed as a result of those energies computed at different methods provides different energies¹⁵² Figure 9 shows the relative population computed at TSPP¹⁵⁵-GD3/def2-TZVP level of theory. At cold temperatures, strongly dominate the chiral structure with symmetry C_1 and depicted in Figure 1(a,b). At hot temperatures, the dominant structure is a chiral helix-type structure depicted in Figure 1(k,l) located at 4.70 kcal/mol Gibbs free energy above the putative global minimum. Also, at SP CCSD(T) level, it is located at high energy above the global minimum. The relative population employing this functional does not follow the trend of energetic ordering at CCSD(T) level of theory. The above discussion shows that the probability of occurrence is sensitive to the functional.

C. Enantiomerization Energy Barrier at Finite Temperature.

The process in which pair of chiral molecules or enantiomers undergo to the conversion of one enantiomer into the other is referred to as enantiomerization. Enantiomers each have the same free energy and equal probability of occurrence, as shown in Figure 4 The extent of interconversion of enantiomers depends on the energy barriers to enantiomerization. Moreover, this energy barrier determines if an enantiomer can be resolved at temperature T and defines its configurational stability. There are cases where the enantiomerization is undesirable; for example, many drugs are related to chirality, and frequently only one of the enantiomers shows the desired effect while the other shows undesirable effects, moreover chiral molecules with high charge-carrier mobility and fluorescence quantum yield needs high energy barriers of enantiomerization.¹⁵⁶

Figure 5a shows the computed enantiomerization energy barrier (energy activation (E_{ae}))

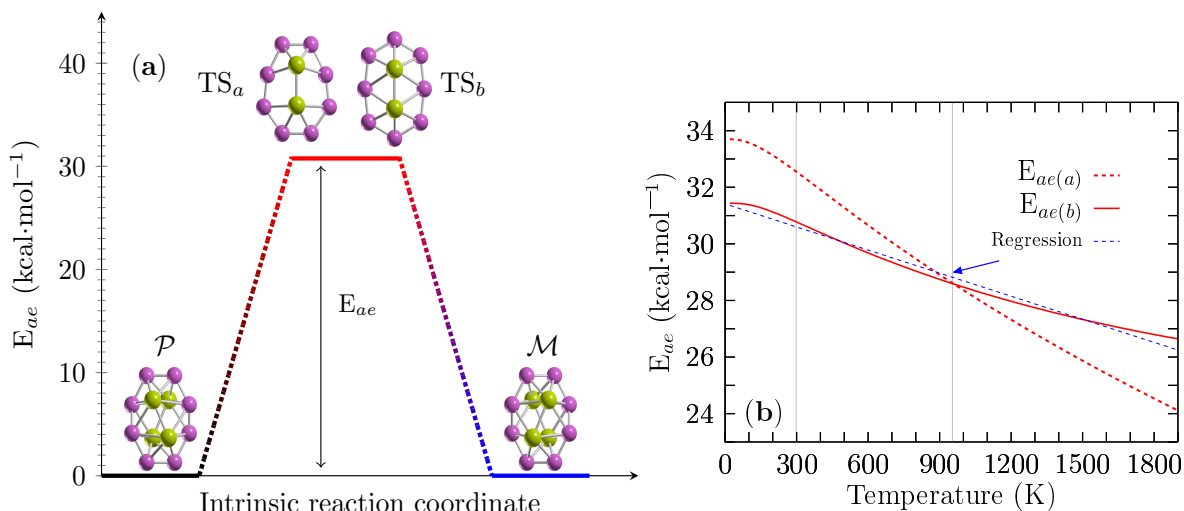


FIG. 5: (Color online) On panel (a), There are two transition states close in energy, TS_a and TS_b depicted in panel (a) and two possible intrinsic reaction coordinates (see movies in Supplementary Material): Route(a): Computed activation energy ($E_{ae(a)}$) of $32.5 \text{ kcal}\cdot\text{mol}^{-1}$. Route(b): Computed activation energy ($E_{ae(b)}$) of $30.77 \text{ kcal}\cdot\text{mol}^{-1}$. between \mathcal{P} and \mathcal{M} chiral Be_4B_8 clusters at room temperature. The energy barrier for interconversion is equal to each other at temperature T , (Temperature barrier-barrier T_{bb} point), which implies the velocity of reaction of both mechanism are equal. For the case of chiral Be_4B_8 T_{bb} is located at 954 K. In panel (b) The $E_{ae(a)}$ is depicted in red dashed line, The $E_{ae(b)}$ is depicted red solid line for temperatures ranging from 20 to 1900 K. At 954 K. The blue-dashed line on panel (b) represents a regression linear in the computed data of the energy barrier $E_{ae(b)}$ depicted in the red solid line in panel (b) its correlation coefficient is -0.9925. Harmonic frequency calculations were employed to make sure that the optimized transition states possess exactly one imaginary frequency.

or Gibbs free activation energy (ΔG^\ddagger) of the pair of enantiomers \mathcal{P} and \mathcal{M} of Be_4B_8 cluster that has only a single-step for two mechanisms of reaction whose energy barriers are energetically similar. The transition states (TS_a , TS_b) depicted in Figure 5a, are achiral sandwich-type structures in which the borons form a planar ring with each of the Be-Be dimers capping the top and bottom, and they are aligned parallel to the major axis of the boron ellipse. The main difference between both of them is a shift of ring position concerning the Be-Be dimers. The energy barriers of TS_a and TS_b are 32.50 and 30.77 kcal/mol, respectively, and indicates that Be_4B_8 enantiomers are stable at room temperature. Those

energy barriers height are similar to that of computed energy barrier height in $\text{Au}_{38}(\text{SR})_{24}$,¹⁵⁷ clusters that lie in the range of 29.9 to 34.5 kcal/mol. The energy of enantiomerization, $E_{ea(a)}$ and $E_{ea(b)}$ corresponding to the TS_a and TS_b for temperatures ranging from 20 to 1900 K are displayed in Figure 5b respectively. The $E_{ea(a)}$ is depicted in a red dashed line, whereas the $E_{ea(b)}$ is depicted in a red solid line. Analysis of the results leads to an interesting observation: In Figure 5b, one can see that there is a barrier-barrier temperature point (T_{bb}) located at 954 K where the energy barriers of both mechanisms are equal to each other. At T_{bb} , the probability that reaction takes one path or another is 50/50% which implies that the velocities of reaction for both reaction mechanism are equal to each other. Below the temperature of 954 K, the reaction path b (TS_b) is more favorable than reaction path a (TS_a), and vice-versa for temperatures above 954 K. In Figure 5b. is shows that the energy barrier $E_{ea(b)}$ decreases linearly in the temperature range from 200 to 740 K. Below 200 K and in temperatures ranging from 740 to 1900 K; the energy barrier behavior is non-linear. To make it clearer, a line depicted in the blue dashed line in Figure 11 appendix C overlapping to energy barrier in the temperature range 200 to 740 K. Equation 9 was found by the linear regression, with correlation coefficients -0.9925, of the energy barrier depicted in a red solid line in Figure 5b.

$$\Delta G^\ddagger = 31.41 - 0.00271188 \cdot T \quad (9)$$

In Equation 9, T is the temperature, and it describes approximately the energy barrier in all ranges of temperature. It is depicted in the blue dashed line of Figure 5b. Evaluating Equation 9 with $T=298.15$ K gives 30.59 kcal/mol, just very close to the computed value of 30.77 kcal/mol. The first term of the Equation 9 is enthalpy, and the second one is the entropic term. The computed values of ΔG , ΔH , ΔS , and the percentage of contribution of ΔS to energy barrier are summarized in Table II for some temperature values. Analysis of results shown in Table II leads that the enthalpy term is too large compared with the entropic term shown in row 3 and row 4 of Table II, respectively, and evaluated in ranging temperatures given in row 1 of Table II. In row five of Table II is given the percentage in which the energy barrier decreases as a function of temperature and due to entropic term considering as reference one hundred percent when the energy barrier is computed at $T=0$. Notably, the composition of the energy barrier is enthalpic and is too high in all ranges of temperature. We concluded that the interconversion between enantiomers is

thermodynamically unfavorable in all ranges of temperature based on our computations. At hot temperatures, the energy barrier still is too high, and the most significant entropic contribution is not more than 15.54%. Similar results are obtained for the TS_b .

TABLE II: Approximate, energy barrier, enthalpy, entropy terms, and the percentage in which the energy barrier decreases, considering the reference of one hundred percent when the energy barrier is computed at $T=0$. The lowering of the energy barrier is due to entropic terms. ($\Delta S \cdot T$) The highest value is 26.52% at hot temperatures, this leads to the observation that the composition of the barrier is at least is 84.4% enthalpic in all ranges of temperature.

Temperature (K)	ΔG	ΔH	$\Delta S \cdot T$	%(Decrease)
0	31.41	31.41	0.0	0.0
300	30.60	31.41	-0.81	2.58
600	29.79	31.41	-1.62	5.17
900	28.97	31.41	-2.44	7.76
1200	28.16	31.41	-3.25	10.35
1500	27.35	31.41	-4.06	12.94
1800	26.53	31.41	-4.88	15.53

D. Energy Barrier between Chiral and Achiral Structures at Finite Temperature.

Figure 6a displays the height of energy barrier interconversion at room temperature between the chiral \mathcal{P}/\mathcal{M} structures shown in Figure 1(1,2), and achiral structure depicted in Figure 17. Remarkable, these structures coexist at the dominant solid-solid transformation point located at 739 K, and according to the probability of occurrence, at hot temperatures, the achiral structure is the putative global minimum. Furthermore, the endergonic to an exergonic temperature point, T_{ee} , is defined here as the temperature where the reaction type change from an endergonic to an exergonic and in this Be_4B_8 clusters it coincides with the solid-solid transformation point. When these two points coincide, at least two structures coexist, and there is a change of type reaction from endergonic to an exergonic or vice-versa. For the interconversion between those structures, the height of the energy barrier at room

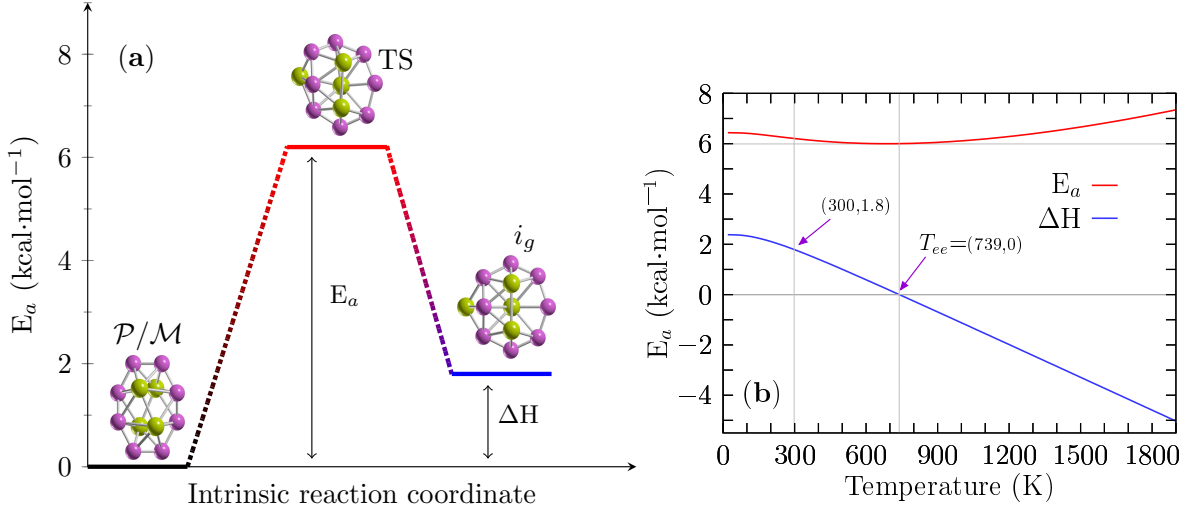


FIG. 6: (Color online) On panel (a), The height of energy barrier for interconversion (E_a) is 6.20 kcal·mol⁻¹ between \mathcal{P} or \mathcal{M} chiral and achiral structures (see Figure 17) of Be_4B_8 clusters at room temperature. On panel (b), the E_a is depicted in the red solid line, and the enthalpy of formation (ΔH) depicted in blue solid line for temperatures ranging from 20 to 1900 K. The ΔH is zero at $T=739$ K and 1.8 kcal/mol at $T=300$ K. Notice, E_a has a minimum located at 739 K.

temperature is 6.20 kcal/mol, and the enthalpy of formation (ΔH) is 1.8 kcal/mol. The TS is depicted in Figure 6a, it is also a sandwich type structure formed by a distorted circular ring in which the Be-Be dimers are capping each faces of the ring, it has similar structure to isomer i_7 depicted in Figure 1(g). Figure 6b shows the height of the energy barrier for chiral and achiral structures depicted in a red solid line, the enthalpy of formation (ΔH) for the same structures is depicted in a solid blue line for temperatures ranging from 20 to 1900 K. An analysis of ΔH in Figure 6b, shows that the reaction process is endothermic for temperatures ranging from 20 to 739 K because the ΔH is positive. At the temperature of 739 K, the ΔH is zero, which implies that the chiral structure with C_1 symmetry and achiral (i_7) structure with C_1 symmetry coexist. The above discussion is in good agreement with the computed point T_{ss-1} located at 739 K displayed in Figure 4a, and according to the probability occurrence, at this point, the chiral and achiral structures coexist. Furthermore, in this temperature point, the height of the energy barrier, depicted in the red-solid line Figure 6b, has a minimum value of 6.0 kcal/mol. At temperatures above 739 K, the reaction process is exothermic due to the ΔH is negative, and the height of the energy barrier starts

to increase slowly. Analysis of results in more detail leads to several observations. The reaction process is endothermic up to 739 K, which implies the absorption of energy, and the chiral structures strongly dominate as the putative global minimum. At temperatures of 739 K, the chiral and not chiral structures coexist. At temperatures above 739 K, the reaction process is exothermic, which implies a heat of reaction, and the non-chiral structures weakly dominate as the putative global minimum. Based on the ΔH behavior in all ranges of temperature, we point out that the reaction is an entropic-driven process due to that type of reaction change from endothermic to exothermic as the temperature increases.

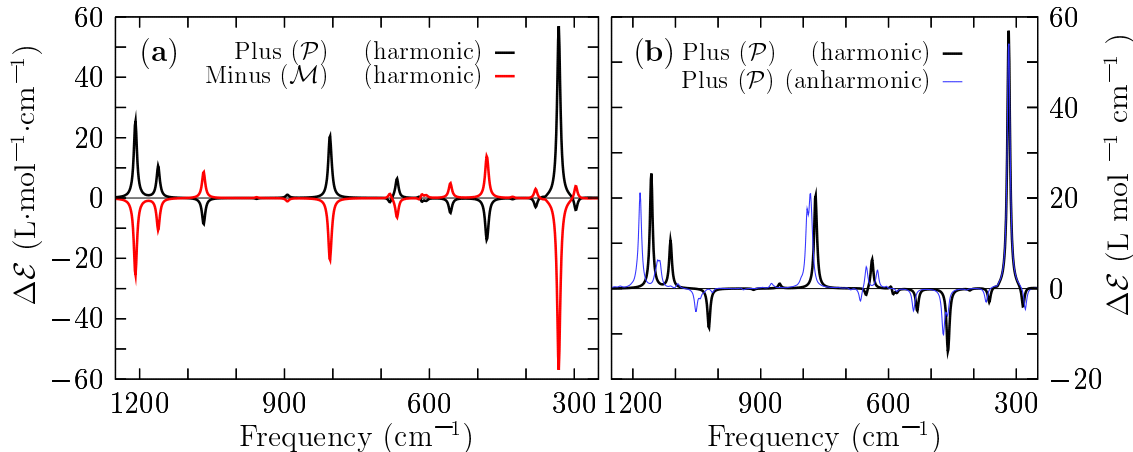


FIG. 7: Panel (a) Shows a comparison of the VCD spectrum for frequencies ranging from 1250-250 cm^{-1} , of the lowest energy \mathcal{P} and \mathcal{M} enantiomers and in Panel (b) it shows a comparison of the VCD-harmonic spectrum and VCD-anharmonic spectrum to estimate the importance of anharmonicities of the Be_4B_8 chiral cluster. The anharmonic vibrational spectrum is depicted in the solid blue line, together with the harmonic vibrational spectrum depicted in solid black line for the lowest energy enantiomers \mathcal{P} . A scale factor of 0.96 is applied to shift the harmonic spectrum to overlay on anharmonic spectrum. The spectra are results of a convolution of a Lorentzian shape profile with FWHM of 20 cm^{-1} with the computed discrete frequency intensities. The x-axis is given the frequency in cm^{-1} and in y-axis is given in units of molar absorptivity ($\Delta\mathcal{E}$)

E. VCD and IR spectra

Figure 7a. shows a comparison of the VCD harmonic spectra corresponding to \mathcal{P} and \mathcal{M} lowest energy structures depicted in solid black- and red lines, respectively. They show a mirror image relationship, thereby ensuring that the two structures are non-superposable. The computed VCD spectrum (\mathcal{P} structure) is characterized by five main peaks located at frequencies of 330 cm^{-1} , 481 cm^{-1} , 802 cm^{-1} , 1062 cm^{-1} , and 1208 cm^{-1} respectively. The largest peak positive intensity is located at 330 cm^{-1} , and it corresponds to the stretching of the two Be-Be dimers that capped the distorted boron ring. Next, a transition located at 481 cm^{-1} is the largest negative and is attributed to bending of the boron distorted ring, a kind of breathing motion. The peaks located in the region 1062 cm^{-1} to 1208 cm^{-1} corresponds to ring boron stretching. The harmonic approximation works if the potential energy is parabolic and it fails¹⁵⁸ as the temperature increases due to anharmonic effects¹⁵⁸ Under harmonic approximation, strongly anharmonic systems are not well described^{159,160} For high temperatures above 0.7...0.8 melting temperature, explicit anharmonic contributions become relevant,¹⁶¹ moreover, we have to consider if the cluster whether or not it is highly strongly anharmonic. To estimate the importance of anharmonicities of the Be_4B_8 chiral cluster, we show, In panel (b) of Figure 7b the anharmonic VCD spectra that is depicted in solid blue line, and for ease comparison overlaying with the harmonic vibrational spectrum depicted in solid black line, both of them computed for \mathcal{P} lowest energy structure, and employing Gaussian code.¹²⁶ A shifting factor of 0.96 is applied to shift the harmonic spectrum to overlaying the anaharmonic spectrum. We found that the frequency shift is 14 cm^{-1} towards to high energy. A comparison of two spectra dispalyed in Figure 7b shows that The computed harmonic and anharmonic spectra are in very good agreement. In fact, most of the peaks are correctly computed employing the harmonic approximation. In the low range of energy the harmonic peaks and anharmonic peaks agree well, however, there are slightly discrepancies in the region 1100 cm^{-1} to 1200 cm^{-1} , nevertheless, in this study the computations of the thermodynamic properties and VCD spectra under the harmonic approximation yield reliable results enough to describe the non-strongly anharmonic Be_4B_8 chiral cluster. Additionally, the Figure 12, appendix D show the IR spectra computed under harmonic and anharmonic approximations. The IR-harmonic spectrum is depicted in solid black line, whereas, the IR-anharmonic spectrum is depicted in solid red line. A shift-

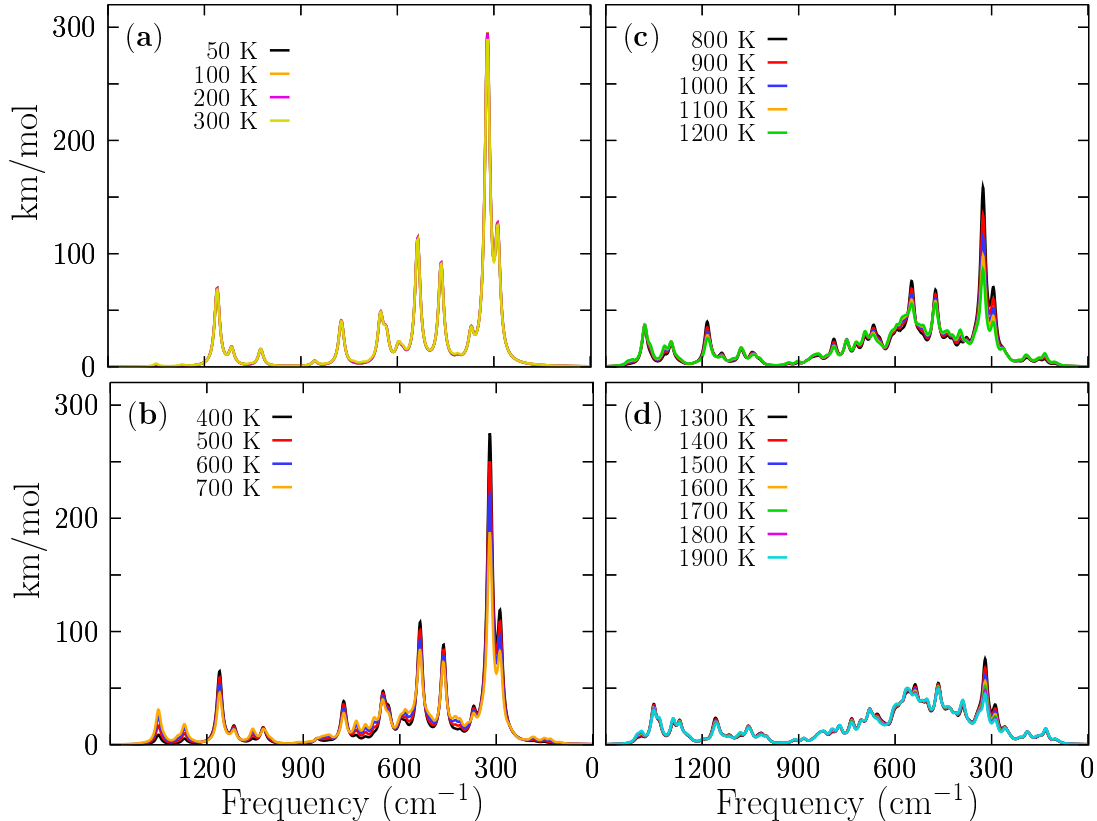


FIG. 8: The dependent temperature IR Boltzmann-spectra-weighted of the \mathcal{P} Be_4B_8 ensemble computed at the PBE0-D3/def2-TZVP level of theory computed in frequency range of 1500 to 1 cm^{-1} . Three similar chiral conformers with C_1 , C_2 and D_2 symmetries which correspond to 96.3% of the Boltzmann distribution, strongly dominate the IR Boltzmann-spectra-weighted in temperature form 0 to 1200 K. The IR Boltzmann-spectra-weighted for temperaturass ranging: in panels (a) 50-300K, (b) 400-700, (c) 800-1200, and (d) 1300-1900 K. At temperatures below 300 K, the amplitud of spectra are constant in good agreement of the realtive population. At temperature above 300 K the magnitude of the spectrum decreases exponentially until to 1200 K. The spectra was computed employing a Lorentzian with half-widths at half-maximum of 20 cm^{-1} . The computed frequencies were multiplied with a scaling factor of 0.96. The x-axis is given the frequency and y-axis is IR intensities in km/mol.

ing factor of 0.96 is applied to match the IR-harmonic spectrum over the IR-anharmonic spectrum. Comparing both spectra, it can see that the spectra match over a large range of frequencies. From the above mentioned we infer that the IR spectra under harmonic approx-

imation yield valid results. Regarding dependent-temperature VCD spectra, the Boltzmann weighted overlapping to yield a total VCD spectrum at all ranging temperatures is zero because the Boltzmann ensemble is composed of achiral structures and an equal mixture of both \mathcal{P} and \mathcal{M} enantiomers, which implies that the Boltzmann ensemble is racemic. Any chiroptical response in the Be_4B_8 cluster is going to be null. The exhaustive exploration of potential and free energy surface revealed that there are twenty two isomers within an energy range of 9.2 kcal/mol, six of which are chiral structures, with symmetries C_1 , C_2 , D_2 respectively, and were within 1 kcal/mol. Moreover, these structures compose 98% of relative population at room temperature. With the aim to compute Boltzmann weighting IR spectra, those structures which only differs on symmetries has to be taken into account. The IR spectra, in comparison to VCD spectra, is not null. Figure 8 shows the IR spectra for temperatures ranging from 50 to 1900 K. The IR spectrum is composed of five peaks. The largest peak intensity is located 330 cm^{-1} frequency axis it corresponds to the alternating stretching of the two Be-Be dimers that capped the distorted boron ring, and it is a mode that contributes to interconversion between P and M structures, The other four modes are related to compression/expansion of the boron ring.

Figure 8a display the IR spectra for temperatures ranging from 50 to 300 K, in this range, the IR spectra is strongly dominated by the spectrum of the lowest energy pair of enantiomers with C_1 symmetry, and further the IR intensities remain constants in all range of temperatures. The above mentioned, is in agreement with the relative population depicted in Figure 4a where the probability of occurrence of the pair of enantiomers with symmetry C_1 strongly dominate. We have to consider that the contribution to IR spectra of the four enantiomers with C_2 and D_2 symmetries for temperature ranging from 20 to 300 K is equal to the IR spectrum with symmetry C_1 , and there is not presence of other structure. Thus at room temperature all molecular properties, except for the chiral properties, are attributable to the lowest energy pair of enantiomers, depicted in Figure 1(a,b). Panel (b) of Figure 8 shows the IR spectra for temperature ranging from 400 to 700 K. The IR intensities start with exponential decay, in agreement with the probability of occurrence of the lowest pair of enantiomers of Figure 4a. There is a little contribution from other isomers, but not enough to change/alter the IR spectrum. Thus the shape of IR spectrum remains equal to IR spectrum at cold temperatures. The IR spectra for temperatures ranging from 800 to 1200 K are shown in Figure 8c, the largest contribution of a particular isomers is less than 17%

thus the largest peak of IR spectra trend to be neglected. Panel (d) in Figure 8 displays that the IR spectra is almost null, thus at hot temperatures the IR spectra is neglected because of almost all contributions of the isomers to IR spectrum are around 10%.

F. Molecular Dynamics

We performed a Born-Oppenheimer molecular dynamics employing the deMon2K program¹⁶² (deMon2k v. 6.01, Cinvestav, Mexico City 2011) at different temperatures (1200, 1500 and 1800 K), with the aim to gain insights into the dynamical behavior of Be_4B_8 cluster. (See movies in supplementary material) We employed similar parameters that in a previous work. The simulation time was of 25 ps with a step size of 1 fs. For Be_4B_8 cluster we found a dissociation phenomena when the temperature is higher than 1500 K, at 1800 K the dissociation process is stronger, while at 1200 K there is no dissociation. When at temperature T , a cluster dissociate the melting point temperature is lower than temperature of dissociation.^{33,163}

IV. CONCLUSIONS

For the first time, to our knowledge and from our results, we found that the chiral cluster Be_4B_8 is the lowest energy structure in ranging temperatures from 0 to 739 K. We initially sampling the potential energy surface with 2400 candidates of neutral Be_4B_8 structures, and with an efficient cascade type algorithm coupled to DFT; We were able to locate twenty-two final isomers within an energy range of 9.2 kcal/mol, six of which are chiral low energy structures with symmetries C_1 , C_2 , and D_2 respectively, as far as we know not yet reported as chiral structures. They are constituted by a sandwich structure type in which the boron atoms form a distorted ellipsoid ring with each Be-Be dimers capping each side of the sandwich. Our findings show that the chirality that exhibits the Be_4B_8 cluster emerges from the Be-Be dimers' mirror position. Additionally, based on the AdNDP analysis and the computed transition state and IRC (see movie Supplementary Information) between \mathcal{P} and \mathcal{M} enantiomers, we can deduce that the Be-Be and Be-B interaction favors the Be_4B_8 to be chiral and energetic minimum structure. According to our calculations, the enantiomerization energy barriers of the transformation \mathcal{P} to \mathcal{M} and \mathcal{M} to \mathcal{P} is equal to each other,

moreover the activation energy between \mathcal{P} to an achiral structure and \mathcal{M} to an achiral structure are equal, thus the Boltzmann ensemble is composed of an equal mixture of \mathcal{M} and \mathcal{P} enantiomers. The enantiomerization energy between the chiral putative global minima in the ranging of temperatures from 20 to 1900 K is mainly composed of enthalpic than entropic term. The entropy-temperature term reduces the interconversion energy barrier like maximum in 28%; thus, the barrier is not influenced significantly by the entropic term. On the other hand, our results show that the energy barrier is 6.20 kcal/mol at room temperature between the lowest energy enantiomer (\mathcal{P}/\mathcal{M}) and the first achiral structure located at 1.79 kcal/mol at 298.15 K. The barrier does not increase significantly neither at cold temperatures nor at hot temperatures, the barrier high at 20 K is 6.43 kcal/mol. In contrast, it is 7.32 kcal/mol at 1900 K. Remarkably, the interconversion between enantiomers and achiral structure is more favored than the interconversion between a pair of enantiomers in all ranges of temperature. Furthermore, our results show that in the temperature range from 20 to 738 K, the interconversion between an enantiomer (\mathcal{P}/\mathcal{M}) and the achiral structure is an endothermic type reaction. At the transformation solid-solid point located at 739 K, the enthalpy of reaction is zero, and the energy barrier is a minimum. In this point coexist the \mathcal{P} and \mathcal{M} structures with an achiral structure. At 739 K, above the interconversion between enantiomers-achiral structures are exothermic, which implies the heat of reaction. Notice that the change from endo to exothermic reaction is driven by entropic-temperature term. In this study and for the first time, we defined two novel points on a scale of temperature. a) The first one is the T_{ee} where the change in the reaction type occurs, and b) the second is the T_{bb} where the activation energy of two different reaction mechanisms are equal to each other, so the reaction rate equals. The energetic ordering of the isomers when we employing the Gibbs free energy computed at 298.15 K with the energy ordering employing the single point CCSD(T) energies computed with DLPNO-CCSD(T), and the energy ordering change just with the interchange of the two achiral structures located at 3.61 kcal/mol and 3.38 kcal/mol above the putative global minimum. Furthermore, Our results on \mathcal{T}_1 diagnostic confirm that energies computed at the DFT level of theory do not contain a large multireference character, so the Be_4B_8 cluster is well characterized. Regarding relative population, our findings show that the putative global minimum that clearly and strongly dominates at cold temperatures is the pair of enantiomers. At 739 K, above, an achiral structure dominates as a putative global minimum with less than 20%. We also show that

the relative population or Boltzmann distribution could depend on the functional and the basis set employed. The energy separation among isomers affects the relative population strongly. The Boltzmann distribution is composed of six isomers at 298.15 K with only different symmetries, and its contribution is approximately 98% thus, at room temperature, the molecular properties are strongly dominated by the pair of enantiomers putative global minimum. We analyzed the effects of the point group symmetry on Gibbs free energy as a function of temperature. The small Gibbs free relative energy differences of 0.41 and 0.81 kcal/mol between different symmetries at 298.15 K are due to rotational entropy that in fact, it is a function of number of symmetry, and it become larger at the temperature increase. This strongly suggests that we need to explore the free energy surface taking into account clusters with low symmetries. The low symmetries trends to dominate as putative global minimum as the temperature increases. For total VCD/IR spectra as a function of temperature, we compute the Boltzmann weighted superposition of each isomer's VCD/IR spectrum that yields a total VCD/IR spectrum. Boltzmann VCD weighted spectra for this particular chiral cluster is null in all range of temperature because in the ensemble P and M enantiomers are present in equal mixture. However, a clear temperature dependence of the Boltzmann IR weighted spectra is driven just by the probability of the putative low-energy isomers in the temperature ranging from 20 to 739 K. At temperature above 739 K, the IR spectra decay strongly, whereas, at a temperature above 1200 K, the IR spectra are almost null. In summary, IR spectra at room temperature are dominated by pair of enantiomers putative global minima, whereas at hot temperatures, the IR spectra are almost null. Our molecular dynamics corroborate that the melting point is located in the temperature ranging from 1400 to 1500 K, because and in accordance with molecular dynamics, the dissociation phenomenon occurs at 1500 K, and the melting point is located below this point. As future work, the inclusion of anharmonic effects should be taken into account also the relative population at CCSDT(T) level of theory is going to be calculated. The melting point also should be computed. At finite temperature the entropy is maximized, taking into account this, a future project is a implementation of an algorithm to search on the free energy surface employing the entropy as an objective function instead of energy. Finally, we point out that in any reaction, the activation energy at finite temperature must be computed considering the reactants and products with non-symmetry (C_1), by reason of the small energy differences dependent on symmetry and temperature (i.e 0.41 kcal/mol for

C₂ at 298.15 K) increase the energy barrier between the reactants and products, hence the velocity of the reaction could be miscalculated. The Boltzmann Optics Full Adder (BOFA) *Python* code supporting the findings of this study is available from the corresponding author upon reasonable request.

V. ACKNOWLEDGMENTS

C. E. B.-G. thanks Conacyt for the Ph.D. scholarship (860052). E. R.-CH. thanks Conacyt for the Ph.D. scholarship (1075701). We are grateful to Dra. Carmen Heras, and L.C.C. Daniel Mendoza for granting us access to their clusters and computational supporting. Computational resources for this work were provided by *ACARUS* through the High-Performance Computing Area of the University of Sonora. Sonora, México. We are also grateful to the computational chemistry laboratory for providing computational resources, *ELBAKYAN* and *PAKAL* supercomputers. Powered@NLHPC: This research was partially supported by the supercomputing infrastructure of the NLHPC (ECM-02) in Chile.

VI. CONFLICTS OF INTEREST

The authors declare no conflict of interest.

VII. FUNDING

This research received no external funding.

VIII. SUPPLEMENTARY MATERIALS

The following are available online at [IRC route A](#) [IRC route B](#). All xyz atomic coordinates optimized of the Be₄B₈ cluster at the PBE0-D3/def2-TZVP/Freq.

IX. ABBREVIATIONS

The following abbreviations are used in this manuscript:

DFT	Density Functional Theory
CCSD(T)	Coupled Cluster Single-Double and perturbative Triple
DLPNO-CCSD(T)	Domain-based Local Pair Natural Orbital Coupled-Cluster Theory
ZPE	Zero-Point Energy
VCD	Vibrational Circular Dichroism
IR	Vibrational Infrared Spectrum
BOFA	Boltzmann-Optics-Full-Ader code
GALGOSON	Global Genetic Algorithm of University of Sonora
SSh	Sandwich-Structure-Hollow
AdNDP	Adaptive Natural Density Partitioning

* email:sollebac@gmail.com, josecabellos@uson.mx

- ¹ T. Kondo, Science and technology of advanced materials **18**, 780 (2017), ISSN 1468-6996, URL <https://doi.org/10.1080/14686996.2017.1379856>.
- ² S. Pan, J. Barroso, S. Jalife, T. Heine, K. R. Asmis, and G. Merino, Accounts of Chemical Research **52**, 2732 (2019), pMID: 31487150, <https://doi.org/10.1021/acs.accounts.9b00336>, URL <https://doi.org/10.1021/acs.accounts.9b00336>.
- ³ N. Kabay, M. Bryjak, and N. Hilal, *Boron Separation Processes* (Elsevier Science, 2015), ISBN 9780444634658, URL <https://books.google.com.mx/books?id=HCItBAAAQBAJ>.
- ⁴ T. Kheshti, Z. Mahdavifar, and S. Noorizadeh, Journal of Molecular Liquids **328**, 115389 (2021), ISSN 0167-7322, URL <https://www.sciencedirect.com/science/article/pii/S016773222100115X>.
- ⁵ H. DeFrancesco, J. Dudley, and A. Coca, *Boron Chemistry: An Overview* (ACS Publications, 2016), chap. 1, pp. 1–25, <https://pubs.acs.org/doi/pdf/10.1021/bk-2016-1236.ch001>, URL <https://pubs.acs.org/doi/abs/10.1021/bk-2016-1236.ch001>.
- ⁶ H.-J. Zhai, Y.-F. Zhao, W.-L. Li, Q. Chen, H. Bai, H.-S. Hu, Z. A. Piazza, W.-J. Tian, H.-G. Lu, Y.-B. Wu, et al., Nature Chemistry pp. 727–731 (2014), URL <https://doi.org/10.1038/nchem.1999>.

- ⁷ Z. A. Piazza, H.-S. Hu, W.-L. Li, Y.-F. Zhao, J. Li, and L.-S. Wang, *Nature Reviews Chemistry* **1**, 0071 (2017), <https://doi.org/10.1038/s41570-017-0071>, URL <https://doi.org/10.1038/s41570-017-0071>.
- ⁸ B. Kiran, S. Bulusu, H.-J. Zhai, S. Yoo, X. C. Zeng, and L.-S. Wang, *Proceedings of the National Academy of Sciences* **102**, 961 (2005), ISSN 0027-8424, <https://www.pnas.org/content/102/4/961.full.pdf>, URL <https://www.pnas.org/content/102/4/961>.
- ⁹ X. Dong, S. Jalife, A. Vásquez-Espinal, E. Ravell, S. Pan, J. L. Cabellos, W.-y. Liang, Z.-h. Cui, and G. Merino, *Angewandte Chemie International Edition* **57**, 4627 (2018), <https://onlinelibrary.wiley.com/doi/pdf/10.1002/anie.201800976>, URL <https://onlinelibrary.wiley.com/doi/abs/10.1002/anie.201800976>.
- ¹⁰ Y.-J. Wang, Y.-F. Zhao, W.-L. Li, T. Jian, Q. Chen, X.-R. You, T. Ou, X.-Y. Zhao, H.-J. Zhai, S.-D. Li, et al., *The Journal of Chemical Physics* **144**, 064307 (2016), <https://doi.org/10.1063/1.4941380>, URL <https://doi.org/10.1063/1.4941380>.
- ¹¹ J. Lv, Y. Wang, L. Zhang, H. Lin, J. Zhao, and Y. Ma, *Nanoscale* **7**, 10482 (2015), URL <http://dx.doi.org/10.1039/C5NR01659B>.
- ¹² Z. A. Piazza, H.-S. Hu, W.-L. Li, Y.-F. Zhao, J. Li, and L.-S. Wang, *Nature Communications* **1**, 3113 (2014), <https://doi.org/10.1038/ncomms4113>, URL <https://doi.org/10.1038/ncomms4113>.
- ¹³ W.-L. Li, Y.-F. Zhao, H.-S. Hu, J. Li, and L.-S. Wang, *Angewandte Chemie International Edition* **53**, 5540 (2014), <https://onlinelibrary.wiley.com/doi/pdf/10.1002/anie.201402488>, URL <https://onlinelibrary.wiley.com/doi/abs/10.1002/anie.201402488>.
- ¹⁴ W. An, S. Bulusu, Y. Gao, and X. C. Zeng, *The Journal of Chemical Physics* **124**, 154310 (2006), <https://doi.org/10.1063/1.2187003>, URL <https://doi.org/10.1063/1.2187003>.
- ¹⁵ X. Dong, S. Jalife, A. Vásquez-Espinal, J. Barroso, M. Orozco-Ic, E. Ravell, J. L. Cabellos, W.-y. Liang, Z.-h. Cui, and G. Merino, *Nanoscale* **11**, 2143 (2019), URL <http://dx.doi.org/10.1039/C8NR09173K>.
- ¹⁶ L.-Y. Feng, J.-C. Guo, P.-F. Li, and H.-J. Zhai, *Chemistry - An Asian Journal* **15**, 1094 (2020), <https://onlinelibrary.wiley.com/doi/pdf/10.1002/asia.201901640>, URL <https://onlinelibrary.wiley.com/doi/abs/10.1002/asia.201901640>.
- ¹⁷ Q. Chen, W.-L. Li, Y.-F. Zhao, S.-Y. Zhang, H.-S. Hu, H. Bai, H.-R. Li, W.-

- J. Tian, H.-G. Lu, H.-J. Zhai, et al., *ACS Nano* **9**, 754 (2015), pMID: 25517915, <https://doi.org/10.1021/nm506262c>, URL <https://doi.org/10.1021/nm506262c>.
- ¹⁸ O. Yañez, D. Inostroza, B. Usuga-Acevedo, A. Vásquez-Espinal, R. Pino-Rios, M. Tabilo-Sepulveda, J. Garza, J. Barroso, G. Merino, and W. Tiznado, *Theoretical Chemistry Accounts* **139**, 139 (2020), <https://doi.org/10.1007/s00214-020-2548-5>, URL <https://doi.org/10.1007/s00214-020-2548-5>.
- ¹⁹ Q. Chen, T.-T. Chen, H.-R. Li, X.-Y. Zhao, W.-J. Chen, H.-J. Zhai, S.-D. Li, and L.-S. Wang, *Nanoscale* **11**, 9698 (2019), URL <http://dx.doi.org/10.1039/C9NR01524H>.
- ²⁰ T. B. Tai and M. T. Nguyen, *Chem. Commun.* **52**, 1653 (2016), URL <http://dx.doi.org/10.1039/C5CC09111J>.
- ²¹ J.-C. Guo, L.-Y. Feng, Y.-J. Wang, S. Jalife, A. Vásquez-Espinal, J. L. Cabellos, S. Pan, G. Merino, and H.-J. Zhai, *Angewandte Chemie International Edition* **56**, 10174 (2017), <https://onlinelibrary.wiley.com/doi/pdf/10.1002/anie.201703979>, URL <https://onlinelibrary.wiley.com/doi/abs/10.1002/anie.201703979>.
- ²² G. Merino and T. Heine, *Angewandte Chemie International Edition* **51**, 10226 (2012), <https://onlinelibrary.wiley.com/doi/pdf/10.1002/anie.201206188>, URL <https://onlinelibrary.wiley.com/doi/abs/10.1002/anie.201206188>.
- ²³ J. Jimenez-Halla, R. Islas, T. Heine, and G. Merino, *Angewandte Chemie International Edition* **49**, 5668 (2010), <https://onlinelibrary.wiley.com/doi/pdf/10.1002/anie.201001275>, URL <https://onlinelibrary.wiley.com/doi/abs/10.1002/anie.201001275>.
- ²⁴ G. Martínez-Guajardo, A. P. Sergeeva, A. I. Boldyrev, T. Heine, J. M. Ugalde, and G. Merino, *Chem. Commun.* **47**, 6242 (2011), URL <http://dx.doi.org/10.1039/C1CC10821B>.
- ²⁵ D. Moreno, S. Pan, L. L. Zeonjuk, R. Islas, E. Osorio, G. Martínez-Guajardo, P. K. Chattaraj, T. Heine, and G. Merino, *Chem. Commun.* **50**, 8140 (2014), URL <http://dx.doi.org/10.1039/C4CC02225D>.
- ²⁶ F. Cervantes-Navarro, G. Martínez-Guajardo, E. Osorio, D. Moreno, W. Tiznado, R. Islas, K. J. Donald, and G. Merino, *Chem. Commun.* **50**, 10680 (2014), URL <http://dx.doi.org/10.1039/C4CC03698K>.
- ²⁷ S. Jalife, L. Liu, S. Pan, J. L. Cabellos, E. Osorio, C. Lu, T. Heine, K. J. Donald, and G. Merino, *Nanoscale* **8**, 17639 (2016), 10.1039/C6NR06383G, URL <http://dx.doi.org/10.1039/C6NR06383G>.

- ²⁸ Y.-J. Wang, L.-Y. Feng, and H.-J. Zhai, *Nanoscale Adv.* **1**, 735 (2019), URL <http://dx.doi.org/10.1039/C8NA00256H>.
- ²⁹ G. Martínez-Guajardo, J. L. Cabellos, A. Díaz-Celaya, S. Pan, R. Islas, P. K. Chattaraj, T. Heine, and G. Merino, *Sci. Report* **22**, 11287 (2015), URL <https://www.nature.com/articles/srep11287>.
- ³⁰ F. L. Gu, X. Yang, A.-C. Tang, H. Jiao, and P. von R. Schleyer, *Journal of Computational Chemistry* **19**, 203 (1998), [https://doi.org/10.1002/\(SICI\)1096-987X\(19980130\)19:2;203::AID-JCC13;3.0.CO;2-I](https://doi.org/10.1002/(SICI)1096-987X(19980130)19:2;203::AID-JCC13;3.0.CO;2-I), URL [https://doi.org/10.1002/\(SICI\)1096-987X\(19980130\)19:2<203::AID-JCC13>3.0.CO;2-I](https://doi.org/10.1002/(SICI)1096-987X(19980130)19:2<203::AID-JCC13>3.0.CO;2-I).
- ³¹ X. Yu, C. Xu, and L. Cheng, *Computational and Theoretical Chemistry* **1188**, 112949 (2020), ISSN 2210-271X, URL <https://www.sciencedirect.com/science/article/pii/S2210271X20302498>.
- ³² F. Baletto and R. Ferrando, *Rev. Mod. Phys.* **77**, 371 (2005), URL <https://link.aps.org/doi/10.1103/RevModPhys.77.371>.
- ³³ C. E. Buelna-Garcia, J. L. Cabellos, J. M. Quiroz-Castillo, G. Martinez-Guajardo, C. Castillo-Quevedo, A. de Leon-Flores, G. Anzueto-Sanchez, and M. F. Martin-del Campo-Solis, *Materials* **14** (2021), ISSN 1996-1944, URL <https://www.mdpi.com/1996-1944/14/1/112>.
- ³⁴ J. C. Axtell, L. M. A. Saleh, E. A. Qian, A. I. Wixtrom, and A. M. Spokoiny, *Inorganic Chemistry* **57**, 2333 (2018), ISSN 0020-1669, URL <https://doi.org/10.1021/acs.inorgchem.7b02912>.
- ³⁵ F. Ali, N. S. Hosmane, and Y. Zhu, *Molecules* **25** (2020), ISSN 1420-3049, URL <https://www.mdpi.com/1420-3049/25/4/828>.
- ³⁶ M. F. Hawthorne, *Angewandte Chemie International Edition in English* **32**, 950 (1993), <https://onlinelibrary.wiley.com/doi/pdf/10.1002/anie.199309501>, URL <https://onlinelibrary.wiley.com/doi/abs/10.1002/anie.199309501>.
- ³⁷ L. Pizzorno, *Integrative medicine (Encinitas, Calif.)* **14**, 35 (2015), ISSN 1546-993X, URL <https://pubmed.ncbi.nlm.nih.gov/26770156>.
- ³⁸ Y. Yang, D. Jia, Y.-J. Wang, H.-J. Zhai, Y. Man, and S.-D. Li, *Nanoscale* **9**, 1443 (2017), URL <http://dx.doi.org/10.1039/C6NR09074E>.
- ³⁹ A. R. Oganov and V. L. Solozhenko, *Journal of Superhard Materials* **31**, 285 (2009), ISSN 1934-9408, URL <https://doi.org/10.3103/S1063457609050013>.

- ⁴⁰ E. Fakioglu, Y. Yürüm, and T. Nejat Veziroglu, International Journal of Hydrogen Energy **29**, 1371 (2004), ISSN 0360-3199, URL <https://www.sciencedirect.com/science/article/pii/S0360319904000114>.
- ⁴¹ H. Jiang, Z. Lu, M. Wu, F. Ciucci, and T. Zhao, Nano Energy **23**, 97 (2016), ISSN 2211-2855, URL <https://www.sciencedirect.com/science/article/pii/S2211285516300222>.
- ⁴² P. Liang, Y. Cao, B. Tai, L. Zhang, H. Shu, F. Li, D. Chao, and X. Du, Journal of Alloys and Compounds **704**, 152 (2017), ISSN 0925-8388, URL <https://www.sciencedirect.com/science/article/pii/S0925838817304668>.
- ⁴³ Y. Zhang, Z.-F. Wu, P.-F. Gao, S.-L. Zhang, and Y.-H. Wen, ACS Applied Materials & Interfaces **8**, 22175 (2016), pMID: 27487298, <https://doi.org/10.1021/acsami.6b05747>, URL <https://doi.org/10.1021/acsami.6b05747>.
- ⁴⁴ N. Jiang, B. Li, F. Ning, and D. Xia, Journal of Energy Chemistry **27**, 1651 (2018), ISSN 2095-4956, URL <https://www.sciencedirect.com/science/article/pii/S2095495618300147>.
- ⁴⁵ S. H. Mir, S. Chakraborty, P. C. Jha, J. Wärnå, H. Soni, P. K. Jha, and R. Ahuja, Applied Physics Letters **109**, 053903 (2016), <https://doi.org/10.1063/1.4960102>, URL <https://doi.org/10.1063/1.4960102>.
- ⁴⁶ Z. Huang, S. Wang, R. D. Dewhurst, N. V. Ignat'ev, M. Finze, and H. Braunschweig, Angewandte Chemie International Edition **59**, 8800 (2020), <https://onlinelibrary.wiley.com/doi/pdf/10.1002/anie.201911108>, URL <https://onlinelibrary.wiley.com/doi/abs/10.1002/anie.201911108>.
- ⁴⁷ D. Ayuso, O. Neufeld, A. F. Ordonez, P. Decleva, G. Lerner, O. Cohen, M. Ivanov, and O. Smirnova, Nature Photonics **13**, 866 (2019), ISSN 1749-4893, URL <https://doi.org/10.1038/s41566-019-0531-2>.
- ⁴⁸ D. Ayuso, A. Ordonez, P. Decleva, M. Ivanov, and O. Smirnova, *Polarization of chirality* (2020), 2004.05191.
- ⁴⁹ P. Guo, B. Yang, L. Zhang, and L. Zhao, Chem. Sci. **9**, 5614 (2018), URL <http://dx.doi.org/10.1039/C8SC00344K>.
- ⁵⁰ A. W. Kaspi-Kaneti, J. Barroso, G. Merino, D. Avnir, I. L. Garzón, and I. Tuvi-Arad, The Journal of Organic Chemistry **85**, 15415 (2020), pMID: 33210538, <https://doi.org/10.1021/acs.joc.0c02196>, URL <https://doi.org/10.1021/acs.joc.0c02196>.

- ⁵¹ J. Barroso, J. L. Cabellos, S. Pan, F. Murillo, X. Zarate, M. A. Fernandez-Herrera, and G. Merino, *Chem. Commun.* **54**, 188 (2018), URL <http://dx.doi.org/10.1039/C7CC08191J>.
- ⁵² D. Ebeling, M. Šekutor, M. Stiefermann, J. Tschakert, J. E. P. Dah, R. M. K. Carlson, A. Schirmeisen, and P. R. Schreiner, *Nature Communications* **9**, 2420 (2018), ISSN 2041-1723, URL <https://doi.org/10.1038/s41467-018-04843-z>.
- ⁵³ Z.-h. Cui, W.-s. Yang, L. Zhao, Y.-h. Ding, and G. Frenking, *Angewandte Chemie International Edition* **55**, 7841 (2016), <https://onlinelibrary.wiley.com/doi/pdf/10.1002/anie.201601890>, URL <https://onlinelibrary.wiley.com/doi/abs/10.1002/anie.201601890>.
- ⁵⁴ A. Hermann, N. W. Ashcroft, and R. Hoffmann, *Chemistry – A European Journal* **19**, 4184 (2013), <https://chemistry-europe.onlinelibrary.wiley.com/doi/pdf/10.1002/chem.201203890>, URL <https://chemistry-europe.onlinelibrary.wiley.com/doi/abs/10.1002/chem.201203890>.
- ⁵⁵ L.-Y. Feng, J.-C. Guo, P.-F. Li, and H.-J. Zhai, *Phys. Chem. Chem. Phys.* **20**, 22719 (2018), URL <http://dx.doi.org/10.1039/C8CP04332A>.
- ⁵⁶ L.-H. Han, Y.-J. Wang, and H.-J. Zhai, *New J. Chem.* **45**, 4675 (2021), URL <http://dx.doi.org/10.1039/D0NJ05961G>.
- ⁵⁷ K. Dongliang, S. Weiguo, S. Hongxiao, L. Cheng, and Xiaoyu, *Sci. Rep.* **9**, 14367 (2019), URL <https://www.nature.com/articles/s41598-019-50905-7>.
- ⁵⁸ T. N. Griбанова, R. M. Minyaev, and V. I. Minkin, *Chemical Physics* **522**, 44 (2019), ISSN 0301-0104, URL <https://www.sciencedirect.com/science/article/pii/S0301010418312862>.
- ⁵⁹ T. N. Griбанова, R. M. Minyaev, V. I. Minkin, and A. I. Boldyrev, *Structural Chemistry* **31**, 2105 (2020), ISSN 1572-9001, URL <https://doi.org/10.1007/s11224-020-01606-9>.
- ⁶⁰ H.-R. Li, H. Liu, X.-X. Tian, W.-Y. Zan, Y.-W. Mu, H.-G. Lu, J. Li, Y.-K. Wang, and S.-D. Li, *Phys. Chem. Chem. Phys.* **19**, 27025 (2017), URL <http://dx.doi.org/10.1039/C7CP05179D>.
- ⁶¹ P. Stephens, F. Devlin, and J. Cheeseman, *VCD Spectroscopy for Organic Chemists* (Taylor & Francis, 2012), ISBN 9781439821718, URL <https://books.google.com.mx/books?id=V9BF02cTMZYC>.
- ⁶² P. U. Biedermann, J. R. Cheeseman, M. J. Frisch, V. Schurig, I. Gutman, and I. Agranat, *The Journal of Organic Chemistry* **64**, 3878 (1999), <https://doi.org/10.1021/jo9821325>, URL <https://doi.org/10.1021/jo9821325>.

- ⁶³ A. Aamouche, F. J. Devlin, P. J. Stephens, J. Drabowicz, B. Bujnicki, and M. Mikołajczyk, *Chemistry - A European Journal* **6**, 4479 (2000), URL <https://chemistry-europe.onlinelibrary.wiley.com/doi/abs/10.1002/1521-3765%2820001215%296%3>
- ⁶⁴ V. P. Nicu, A. Mándi, T. Kurtán, and P. L. Polavarapu, *Chirality* **26**, 525 (2014), <https://onlinelibrary.wiley.com/doi/pdf/10.1002/chir.22330>, URL <https://onlinelibrary.wiley.com/doi/abs/10.1002/chir.22330>.
- ⁶⁵ E. Castiglioni, P. Biscarini, and S. Abbate, *Chirality* **21**, E28 (2009), <https://onlinelibrary.wiley.com/doi/pdf/10.1002/chir.20770>, URL <https://onlinelibrary.wiley.com/doi/abs/10.1002/chir.20770>.
- ⁶⁶ J. R. Avilés Moreno, M. M. Quesada Moreno, J. J. López González, R. M. Claramunt, C. López, I. Alkorta, and J. Elguero, *ChemPhysChem* **14**, 3355 (2013), <https://chemistry-europe.onlinelibrary.wiley.com/doi/pdf/10.1002/cphc.201300503>, URL <https://chemistry-europe.onlinelibrary.wiley.com/doi/abs/10.1002/cphc.201300503>.
- ⁶⁷ J. R. Aviles-Moreno, E. Urena Horno, F. Partal Urena, and J. J. López González, *Spectrochimica Acta Part A: Molecular and Biomolecular Spectroscopy* **79**, 767 (2011), ISSN 1386-1425, the Xth International Conference on Molecular Spectroscopy, URL <https://www.sciencedirect.com/science/article/pii/S1386142510004415>.
- ⁶⁸ F. Partal Ureña, J. R. Avilés Moreno, and J. J. López González, *The Journal of Physical Chemistry A* **112**, 7887 (2008), <https://doi.org/10.1021/jp801099e>, URL <https://doi.org/10.1021/jp801099e>.
- ⁶⁹ T. Huet, J.-R. Aviles Moreno, O. Pirali, M. Tudorie, F. Partal Ureña, and J.-J. Lopez Gonzalez, *Journal of Quantitative Spectroscopy and Radiative Transfer* **113**, 1261 (2012), ISSN 0022-4073, three Leaders in Spectroscopy, URL <https://www.sciencedirect.com/science/article/pii/S0022407311003785>.
- ⁷⁰ G. Yang and Y. Xu, *Vibrational Circular Dichroism Spectroscopy of Chiral Molecules* (Springer Berlin Heidelberg, Berlin, Heidelberg, 2011), pp. 189–236, ISBN 978-3-642-18104-7, URL https://doi.org/10.1007/128_2010_86.
- ⁷¹ L. A. Nafie, J. C. Cheng, and P. J. Stephens, *Journal of the American Chemical Society* **97**, 3842 (1975), <https://doi.org/10.1021/ja00846a061>, URL <https://doi.org/10.1021/ja00846a061>.
- ⁷² E. C. Sherer, C. H. Lee, J. Shpungin, J. F. Cuff, C. Da, R. Ball, R. Bach, A. Crespo, X. Gong, and C. J. Welch, *Journal of Medicinal Chemistry* **57**, 477 (2014), PMID: 24383452,

- <https://doi.org/10.1021/jm401600u>, URL <https://doi.org/10.1021/jm401600u>.
- ⁷³ P. J. Stephens, F. J. Devlin, and J.-J. Pan, *Chirality* **20**, 643 (2008), <https://onlinelibrary.wiley.com/doi/pdf/10.1002/chir.20477>, URL <https://onlinelibrary.wiley.com/doi/abs/10.1002/chir.20477>.
- ⁷⁴ E. Dzib, J. L. Cabellos, F. Ortíz-Chi, S. Pan, A. Galano, and G. Merino, *International Journal of Quantum Chemistry* **119**, e25686 (2019), <https://onlinelibrary.wiley.com/doi/pdf/10.1002/qua.25686>, URL <https://onlinelibrary.wiley.com/doi/abs/10.1002/qua.25686>.
- ⁷⁵ J. Kubicki and H. Watts, *Minerals* **9**, 141 (2019), ISSN 2075-163X, URL <http://dx.doi.org/10.3390/min9030141>.
- ⁷⁶ M. R. Fagiani, X. Song, P. Petkov, S. Debnath, S. Gewinner, W. Schöllkopf, T. Heine, A. Fielicke, and K. R. Asmis, *Angewandte Chemie International Edition* **56**, 501 (2017), <https://onlinelibrary.wiley.com/doi/pdf/10.1002/anie.201609766>, URL <https://onlinelibrary.wiley.com/doi/abs/10.1002/anie.201609766>.
- ⁷⁷ C. E. Buelna-García, E. Robles-Chaparro, T. Parra-Arellano, J. M. Quiroz-Castillo, T. del Castillo-Castro, G. Martínez-Guajardo, C. Castillo-Quevedo, A. de León-Flores, G. Anzueto-Sánchez, M. F. Martín-del Campo-Solis, et al., *Molecules* **26** (2021), ISSN 1420-3049, URL <https://www.mdpi.com/1420-3049/26/13/3953>.
- ⁷⁸ Z. H. Li and D. G. Truhlar, *Chem. Sci.* **5**, 2605 (2014), URL <http://dx.doi.org/10.1039/C4SC00052H>.
- ⁷⁹ Z. H. Li, A. W. Jasper, and D. G. Truhlar, *Journal of the American Chemical Society* **129**, 14899 (2007), PMID: 17994736, <https://doi.org/10.1021/ja073129i>, URL <https://doi.org/10.1021/ja073129i>.
- ⁸⁰ V. G. Grigoryan and M. Springborg, *Phys. Chem. Chem. Phys.* **21**, 5646 (2019), URL <http://dx.doi.org/10.1039/C9CP00123A>.
- ⁸¹ C. Sutton and S. V. Levchenko, *Frontiers in Chemistry* **8**, 757 (2020), ISSN 2296-2646, URL <https://www.frontiersin.org/article/10.3389/fchem.2020.00757>.
- ⁸² N. D. Mermin, *Phys. Rev.* **137**, A1441 (1965), URL <https://link.aps.org/doi/10.1103/PhysRev.137.A1441>.
- ⁸³ S. Pittalis, C. R. Proetto, A. Floris, A. Sanna, C. Bersier, K. Burke, and E. K. U. Gross, *Phys. Rev. Lett.* **107**, 163001 (2011), URL

- <https://link.aps.org/doi/10.1103/PhysRevLett.107.163001>.
- ⁸⁴ A. Gonis and M. Däne, *Journal of Physics and Chemistry of Solids* **116**, 86 (2018), ISSN 0022-3697, URL <https://www.sciencedirect.com/science/article/pii/S0022369717310442>.
- ⁸⁵ H. Eschrig, *Phys. Rev. B* **82**, 205120 (2010), URL <https://link.aps.org/doi/10.1103/PhysRevB.82.205120>.
- ⁸⁶ A. P. Seitsonen, K. Laasonen, R. M. Nieminen, and M. L. Klein, *The Journal of Chemical Physics* **103**, 8075 (1995), <https://doi.org/10.1063/1.470172>, URL <https://doi.org/10.1063/1.470172>.
- ⁸⁷ D. J. Wales, *Science* **271**, 925 (1996), ISSN 00368075, 10959203, URL <http://www.jstor.org/stable/2889981>.
- ⁸⁸ T. L. Hill, *The Journal of Chemical Physics* **36**, 3182 (1962), <https://doi.org/10.1063/1.1732447>, URL <https://doi.org/10.1063/1.1732447>.
- ⁸⁹ H. Fox, A. P. Horsfield, and M. J. Gillan, *The Journal of Chemical Physics* **124**, 134709 (2006), <https://doi.org/10.1063/1.2184313>, URL <https://doi.org/10.1063/1.2184313>.
- ⁹⁰ P. J. Stephens, *Theoretical Chemistry Accounts* **119**, 5 (2008), ISSN 1432-2234, URL <https://doi.org/10.1007/s00214-006-0190-5>.
- ⁹¹ L. Nafie, *Vibrational Optical Activity: Principles and Applications* (Wiley, 2011), ISBN 9781119977537, URL <https://books.google.com.mx/books?id=7Pvjg-PWvjEC>.
- ⁹² L. A. Nafie, *Annual Review of Physical Chemistry* **48**, 357 (1997), PMID: 9348659, <https://doi.org/10.1146/annurev.physchem.48.1.357>, URL <https://doi.org/10.1146/annurev.physchem.48.1.357>.
- ⁹³ Y. He, B. Wang, R. K. Dukor, and L. A. Nafie, *Applied Spectroscopy* **65**, 699 (2011), PMID: 21740631, <https://doi.org/10.1366/11-06321>, URL <https://doi.org/10.1366/11-06321>.
- ⁹⁴ F. Calvo, *Phys. Chem. Chem. Phys.* **17**, 27922 (2015), URL <http://dx.doi.org/10.1039/C5CP00274E>.
- ⁹⁵ S. J. Teague, *Nature Reviews Drug Discovery* **2**, 527 (2003), URL <https://doi.org/10.1038/nrd1129>.
- ⁹⁶ M. W. C. Dharma-wardana, *Computation* **4** (2016), ISSN 2079-3197, URL <https://www.mdpi.com/2079-3197/4/2/16>.
- ⁹⁷ G. M. Morris, D. S. Goodsell, R. S. Halliday, R. Huey, W. E. Hart, R. K. Belew, and A. J. Olson, *Journal of Computational Chemistry* **19**, 1639 (1998),

- [https://doi.org/10.1002/\(SICI\)1096-987X\(19981115\)19:14;1639::AID-JCC10;3.0.CO;2-B](https://doi.org/10.1002/(SICI)1096-987X(19981115)19:14;1639::AID-JCC10;3.0.CO;2-B),
URL [https://doi.org/10.1002/\(SICI\)1096-987X\(19981115\)19:14;1639::AID-JCC10;3.0.CO;2-B](https://doi.org/10.1002/(SICI)1096-987X(19981115)19:14;1639::AID-JCC10;3.0.CO;2-B).
- ⁹⁸ C. J. Pickard and R. J. Needs, *Journal of Physics: Condensed Matter* **23**, 053201 (2011), URL <https://doi.org/10.1088/0953-8984/23/5/053201>.
- ⁹⁹ S. Kirkpatrick, C. D. Gelatt, and M. P. Vecchi, *Science* **220**, 671 (1983).
- ¹⁰⁰ N. Metropolis, A. W. Rosenbluth, M. N. Rosenbluth, A. H. Teller, and E. Teller, *J. Chem. Phys.* **21**, 1087 (1953), URL <http://scitation.aip.org/content/aip/journal/jcp/21/6/10.1063/1.1699114>.
- ¹⁰¹ Y. Xiang and X. G. Gong, *Phys. Rev. E* **62**, 4473 (2000), URL <http://link.aps.org/doi/10.1103/PhysRevE.62.4473>.
- ¹⁰² Y. Xiang, S. Gubian, B. Suomela, and J. Hoeng, *The R Journal* **5**, 13 (2013), URL <http://journal.r-project.org/archive/2013-1/xiang-gubian-suomela-etal.pdf>.
- ¹⁰³ D. Vlachos, L. Schmidt, and R. Aris, *Z. Phys. D Atom Mol. Cl.* **26**, 156 (1993), ISSN 0178-7683, URL <http://dx.doi.org/10.1007/BF01425649>.
- ¹⁰⁴ V. Granville, M. Krivanek, and J.-P. Rasson, *IEEE Trans. Pattern Anal. Mach. Intell.* **16**, 652 (1994), ISSN 0162-8828.
- ¹⁰⁵ S. Pan, D. Moreno, J. L. Cabellos, J. Romero, A. Reyes, G. Merino, and P. K. Chattaraj, *The Journal of Physical Chemistry A* **118**, 487 (2014), pMID: 24199587, <https://doi.org/10.1021/jp409941v>, URL <https://doi.org/10.1021/jp409941v>.
- ¹⁰⁶ Z.-h. Cui, Y.-h. Ding, J. L. Cabellos, E. Osorio, R. Islas, A. Restrepo, and G. Merino, *Phys. Chem. Chem. Phys.* **17**, 8769 (2015), URL <http://dx.doi.org/10.1039/C4CP05707D>.
- ¹⁰⁷ A. Vargas-Caamal, S. Pan, F. Ortiz-Chi, J. L. Cabellos, R. A. Boto, J. Contreras-Garcia, A. Restrepo, P. K. Chattaraj, and G. Merino, *Phys. Chem. Chem. Phys.* **18**, 550 (2016), URL <http://dx.doi.org/10.1039/C5CP05956A>.
- ¹⁰⁸ A. Vargas-Caamal, J. L. Cabellos, F. Ortiz-Chi, H. S. Rzepa, A. Restrepo, and G. Merino, *Chemistry – A European Journal* **22**, 2812 (2016), <https://chemistry-europe.onlinelibrary.wiley.com/doi/pdf/10.1002/chem.201504016>, URL <https://chemistry-europe.onlinelibrary.wiley.com/doi/abs/10.1002/chem.201504016>.
- ¹⁰⁹ Z.-h. Cui, V. Vassilev-Galindo, J. Luis Cabellos, E. Osorio, M. Orozco, S. Pan, Y.-h. Ding, and G. Merino, *Chem. Commun.* **53**, 138 (2017), URL <http://dx.doi.org/10.1039/C6CC08273D>.
- ¹¹⁰ A. Vargas-Caamal, F. Ortiz-Chi, D. Moreno, A. Restrepo, G. Merino, and J. L. Cabellos,

- Theoretical Chemistry Accounts **134**, 16 (2015), <https://doi.org/10.1007/s00214-015-1615-9>, URL <https://doi.org/10.1007/s00214-015-1615-9>.
- ¹¹¹ E. Flórez, N. Acelas, C. Ibarguen, S. Mondal, J. L. Cabellos, G. Merino, and A. Restrepo, RSC Adv. **6**, 71913 (2016), URL <http://dx.doi.org/10.1039/C6RA15059D>.
- ¹¹² E. Ravell, S. Jalife, J. Barroso, M. Orozco-Ic, G. Hernandez-Juarez, F. Ortiz-Chi, S. Pan, J. L. Cabellos, and G. Merino, Chemistry - An Asian Journal **13**, 1467 (2018), <https://onlinelibrary.wiley.com/doi/pdf/10.1002/asia.201800261>, URL <https://onlinelibrary.wiley.com/doi/abs/10.1002/asia.201800261>.
- ¹¹³ C. Z. Hadad, E. Florez, G. Merino, J. L. Cabellos, F. Ferraro, and A. Restrepo, The Journal of Physical Chemistry A **118**, 5762 (2014), PMID: 24533862, <https://doi.org/10.1021/jp4099045>, URL <https://doi.org/10.1021/jp4099045>.
- ¹¹⁴ M. Saunders, Journal of Computational Chemistry **25**, 621 (2004), <https://onlinelibrary.wiley.com/doi/pdf/10.1002/jcc.10407>, URL <https://onlinelibrary.wiley.com/doi/abs/10.1002/jcc.10407>.
- ¹¹⁵ M. Saunders, Journal of the American Chemical Society **109**, 3150 (1987), <https://doi.org/10.1021/ja00244a051>, URL <https://doi.org/10.1021/ja00244a051>.
- ¹¹⁶ R. Grande-Aztatzi, P. R. Martínez-Alanis, J. L. Cabellos, E. Osorio, A. Martínez, and G. Merino, Journal of Computational Chemistry **35**, 2288 (2014), <https://onlinelibrary.wiley.com/doi/pdf/10.1002/jcc.23748>, URL <https://onlinelibrary.wiley.com/doi/abs/10.1002/jcc.23748>.
- ¹¹⁷ S. Jalife, S. Mondal, J. L. Cabellos, S. Pan, M. A. Mendez-Rojas, I. Fernandez, G. Frenking, and G. Merino, ChemistrySelect **1**, 2405 (2016), <https://chemistry-europe.onlinelibrary.wiley.com/doi/pdf/10.1002/slct.201600525>, URL <https://chemistry-europe.onlinelibrary.wiley.com/doi/abs/10.1002/slct.201600525>.
- ¹¹⁸ S. Mondal, J. L. Cabellos, S. Pan, E. Osorio, J. J. Torres-Vega, W. Tiznado, A. Restrepo, and G. Merino, Phys. Chem. Chem. Phys. **18**, 11909 (2016), URL <http://dx.doi.org/10.1039/C6CP00671J>.
- ¹¹⁹ M. Contreras, S. Pan, M. Orozco-Ic, J. L. Cabellos, and G. Merino, Chemistry - A European Journal **23**, 11430 (2017), <https://chemistry-europe.onlinelibrary.wiley.com/doi/pdf/10.1002/chem.201702413>, URL <https://chemistry-europe.onlinelibrary.wiley.com/doi/abs/10.1002/chem.201702413>.

- ¹²⁰ S. Pan, J. L. Cabellos, M. Orozco-Ic, P. K. Chattaraj, L. Zhao, and G. Merino, *Phys. Chem. Chem. Phys.* **20**, 12350 (2018), URL <http://dx.doi.org/10.1039/C8CP01009A>.
- ¹²¹ P. L. Rodríguez-Kessler, S. Pan, E. Florez, J. L. Cabellos, and G. Merino, *The Journal of Physical Chemistry C* **121**, 19420 (2017), <https://doi.org/10.1021/acs.jpcc.7b05048>, URL <https://doi.org/10.1021/acs.jpcc.7b05048>.
- ¹²² A. N. Alexandrova, A. I. Boldyrev, Y.-J. Fu, X. Yang, X.-B. Wang, and L.-S. Wang, *J. Chem. Phys.* **121**, 5709 (2004), URL <http://scitation.aip.org/content/aip/journal/jcp/121/12/10.1063/1.1783276>.
- ¹²³ F. Murillo, A. Vargas-Caamal, S. Pan, J. L. Cabellos, M. J. Mora-Fonz, A. MuNoz-Castro, A. Restrepo, and G. Merino, *Phys. Chem. Chem. Phys.* **19**, 17088 (2017), URL <http://dx.doi.org/10.1039/C7CP01328K>.
- ¹²⁴ J. L. Cabellos, F. Ortiz-Chi, A. Ramirez, and G. Merino, *Cinvestav-Merida* **1**, 1 (2018).
- ¹²⁵ G. Hernández-Juárez, E. Ravell, J. Arcudia, X. Zarate, Z.-h. Cui, G. Merino, and J. Barroso, *Phys. Chem. Chem. Phys.* **22**, 17344 (2020), URL <http://dx.doi.org/10.1039/D0CP02750B>.
- ¹²⁶ M. J. Frisch, G. W. Trucks, H. B. Schlegel, G. E. Scuseria, M. A. Robb, J. R. Cheeseman, G. Scalmani, V. Barone, B. Mennucci, G. A. Petersson, et al., *Gaussian 09, Revision B.01* (2009).
- ¹²⁷ A. C. Castro, E. Osorio, J. L. Cabellos, E. Cerpa, E. Matito, M. Solà, M. Swart, and G. Merino, *Chemistry-A European Journal* **20**, 4583 (2014), <https://chemistry-europe.onlinelibrary.wiley.com/doi/pdf/10.1002/chem.201304685>, URL <https://chemistry-europe.onlinelibrary.wiley.com/doi/abs/10.1002/chem.201304685>.
- ¹²⁸ C. Adamo and V. Barone, *The Journal of Chemical Physics* **110**, 6158 (1999), <https://doi.org/10.1063/1.478522>, URL <https://doi.org/10.1063/1.478522>.
- ¹²⁹ T. H. J. Dunning and P. J. Hay, in *Methods of Electronic Structure Theory*, edited by H. F. Schaefer-III (Springer US, Plenum, New York, 1977), chap. 1, pp. 1–28.
- ¹³⁰ J. Zhao, L. Wang, F. Li, and Z. Chen, *The Journal of Physical Chemistry A* **114**, 9969 (2010), PMID: 20695630, <https://doi.org/10.1021/jp1018873>, URL <https://doi.org/10.1021/jp1018873>.
- ¹³¹ J.-D. Chai and S.-P. Mao, *Chemical Physics Letters* **538**, 121 (2012), ISSN 0009-2614, URL <https://www.sciencedirect.com/science/article/pii/S000926141200526X>.
- ¹³² L.-L. Pan, J. Li, and L.-S. Wang, *The Journal of Chemical Physics* **129**, 024302 (2008),

- <https://doi.org/10.1063/1.2948405>, URL <https://doi.org/10.1063/1.2948405>.
- ¹³³ T. S. Rush, J. A. Grant, L. Mosyak, and A. Nicholls, *Journal of Medicinal Chemistry* **48**, 1489 (2005), pMID: 15743191, <https://doi.org/10.1021/jm040163o>, URL <https://doi.org/10.1021/jm040163o>.
- ¹³⁴ F. Weigend and R. Ahlrichs, *Phys. Chem. Chem. Phys.* **7**, 3297 (2005), URL <http://dx.doi.org/10.1039/B508541A>.
- ¹³⁵ A. Schafer, C. Huber, and R. Ahlrichs, *The Journal of Chemical Physics* **100**, 5829 (1994), <https://doi.org/10.1063/1.467146>, URL <https://doi.org/10.1063/1.467146>.
- ¹³⁶ S. Grimme, J. Antony, S. Ehrlich, and H. Krieg, *The Journal of Chemical Physics* **132**, 154104 (2010), <https://doi.org/10.1063/1.3382344>, URL <https://doi.org/10.1063/1.3382344>.
- ¹³⁷ T. J. Lee and P. R. Taylor, *International Journal of Quantum Chemistry* **36**, 199 (1989), <https://onlinelibrary.wiley.com/doi/pdf/10.1002/qua.560360824>, URL <https://onlinelibrary.wiley.com/doi/abs/10.1002/qua.560360824>.
- ¹³⁸ D. G. Liakos, Y. Guo, and F. Neese, *The Journal of Physical Chemistry A* **124**, 90 (2020), pMID: 31841627, <https://doi.org/10.1021/acs.jpca.9b05734>, URL <https://doi.org/10.1021/acs.jpca.9b05734>.
- ¹³⁹ D. G. Liakos, M. Sparta, M. K. Kesharwani, J. M. L. Martin, and F. Neese, *Journal of Chemical Theory and Computation* **11**, 1525 (2015), pMID: 26889511, <https://doi.org/10.1021/ct501129s>, URL <https://doi.org/10.1021/ct501129s>.
- ¹⁴⁰ D. Y. Zubarev and A. I. Boldyrev, *Phys. Chem. Chem. Phys.* **10**, 5207 (2008), URL <http://dx.doi.org/10.1039/B804083D>.
- ¹⁴¹ G. Brehm, M. Reiher, B. Le Guennic, M. Leibold, S. Schindler, F. W. Heine-
mann, and S. Schneider, *Journal of Raman Spectroscopy* **37**, 108 (2006), <https://analyticalsciencejournals.onlinelibrary.wiley.com/doi/pdf/10.1002/jrs.1437>, URL <https://analyticalsciencejournals.onlinelibrary.wiley.com/doi/abs/10.1002/jrs.1437>.
- ¹⁴² D. McQuarrie and M. A., *Statistical Mechanics*, Chemistry Series (Harper & Row, 1975), URL <https://books.google.com.bo/books?id=PANRAAAAMAAJ>.
- ¹⁴³ T. Hill, *An Introduction to Statistical Thermodynamics*, Addison-Wesley series in chemistry (Dover Publications, 1986), ISBN 9780486652429, URL <https://books.google.com.vc/books?id=OfNItAEACAAJ>.
- ¹⁴⁴ S. Bhattacharya, D. Berger, K. Reuter, L. M. Ghiringhelli, and

- S. V. Levchenko, *Phys. Rev. Materials* **1**, 071601 (2017), URL <https://link.aps.org/doi/10.1103/PhysRevMaterials.1.071601>.
- ¹⁴⁵ P. Bhumla, M. Kumar, and S. Bhattacharya, *Nanoscale Adv.* **3**, 575 (2021), URL <http://dx.doi.org/10.1039/D0NA00669F>.
- ¹⁴⁶ D. Shortle, *Computational and Theoretical Chemistry* **12**, 1298 (2003), ISSN 1469-896X, URL <https://pubmed.ncbi.nlm.nih.gov/12761401>.
- ¹⁴⁷ A. M. Mendoza-Wilson, R. R. Balandrán-Quintana, and J. L. Cabellos, *Computational and Theoretical Chemistry* **1186**, 112912 (2020), ISSN 2210-271X, URL <http://www.sciencedirect.com/science/article/pii/S2210271X20302127>.
- ¹⁴⁸ D. Schebarchov, F. Baletto, and D. J. Wales, *Nanoscale* **10**, 2004 (2018), URL <http://dx.doi.org/10.1039/C7NR07123J>.
- ¹⁴⁹ B. R. Goldsmith, J. Florian, J.-X. Liu, P. Gruene, J. T. Lyon, D. M. Rayner, A. Fielicke, M. Scheffler, and L. M. Ghiringhelli, *Phys. Rev. Materials* **3**, 016002 (2019), URL <https://link.aps.org/doi/10.1103/PhysRevMaterials.3.016002>.
- ¹⁵⁰ A. Moezzi, M. M. Olmstead, and P. P. Power, *Journal of the American Chemical Society* **114**, 2715 (1992), <https://doi.org/10.1021/ja00033a054>, URL <https://doi.org/10.1021/ja00033a054>.
- ¹⁵¹ M. Zhou, N. Tsumori, Z. Li, K. Fan, L. Andrews, and Q. Xu, *Journal of the American Chemical Society* **124**, 12936 (2002), PMID: 12405806, <https://doi.org/10.1021/ja026257+>, URL <https://doi.org/10.1021/ja026257+>.
- ¹⁵² E. de la Puente, A. Aguado, A. Ayuela, and J. M. López, *Phys. Rev. B* **56**, 7607 (1997), URL <https://link.aps.org/doi/10.1103/PhysRevB.56.7607>.
- ¹⁵³ P. Oswald, K. Desmet, P. Sandra, J. Krupcik, P. Májek, and D. W. Armstrong, *Journal of Chromatography B* **779**, 283 (2002), ISSN 1570-0232, URL <https://www.sciencedirect.com/science/article/pii/S1570023202003963>.
- ¹⁵⁴ J. A. Pople, M. Head-Gordon, and K. Raghavachari, *The Journal of Chemical Physics* **87**, 5968 (1987), <https://doi.org/10.1063/1.453520>, URL <https://doi.org/10.1063/1.453520>.
- ¹⁵⁵ J. Tao, J. P. Perdew, V. N. Staroverov, and G. E. Scuseria, *Phys. Rev. Lett.* **91**, 146401 (2003), URL <https://link.aps.org/doi/10.1103/PhysRevLett.91.146401>.
- ¹⁵⁶ P. Ravat, *Chemistry – A European Journal* **27**, 3957 (2021), <https://chemistry-europe.onlinelibrary.wiley.com/doi/pdf/10.1002/chem.202004488>, URL

- <https://chemistry-europe.onlinelibrary.wiley.com/doi/abs/10.1002/chem.202004488>.
- ¹⁵⁷ S. Malola and H. Häkkinen, *Journal of the American Chemical Society* **141**, 6006 (2019), pMID: 30889350, <https://doi.org/10.1021/jacs.9b01204>, URL <https://doi.org/10.1021/jacs.9b01204>.
- ¹⁵⁸ K. R. Glaesemann and L. E. Fried, *The Journal of Chemical Physics* **123**, 034103 (2005), <https://doi.org/10.1063/1.1954771>, URL <https://doi.org/10.1063/1.1954771>.
- ¹⁵⁹ O. Hellman, P. Steneteg, I. A. Abrikosov, and S. I. Simak, *Phys. Rev. B* **87**, 104111 (2013), URL <https://link.aps.org/doi/10.1103/PhysRevB.87.104111>.
- ¹⁶⁰ G. Grimvall, B. Magyari-Köpe, V. Ozoliņš, and K. A. Persson, *Rev. Mod. Phys.* **84**, 945 (2012), URL <https://link.aps.org/doi/10.1103/RevModPhys.84.945>.
- ¹⁶¹ J. Neugebauer and T. Hickel, *WIREs Computational Molecular Science* **3**, 438 (2013), <https://onlinelibrary.wiley.com/doi/pdf/10.1002/wcms.1125>, URL <https://onlinelibrary.wiley.com/doi/abs/10.1002/wcms.1125>.
- ¹⁶² G. Geudtner, P. Calaminici, J. Carmona-Espíndola, J. M. del Campo, V. D. Domínguez-Soria, R. F. Moreno, G. U. Gamboa, A. Goursot, A. M. Köster, J. U. Reveles, et al., *WIREs Computational Molecular Science* **2**, 548 (2012), <https://onlinelibrary.wiley.com/doi/pdf/10.1002/wcms.98>, URL <https://onlinelibrary.wiley.com/doi/abs/10.1002/wcms.98>.
- ¹⁶³ M. Li, J. Wang, B. Fu, and Q. Hou, *AIP Advances* **5**, 127131 (2015), <https://doi.org/10.1063/1.4939137>, URL <https://doi.org/10.1063/1.4939137>.

Appendix A: Probability of occurrence computed at TPSS-GD3/def2TZVP level of theory.

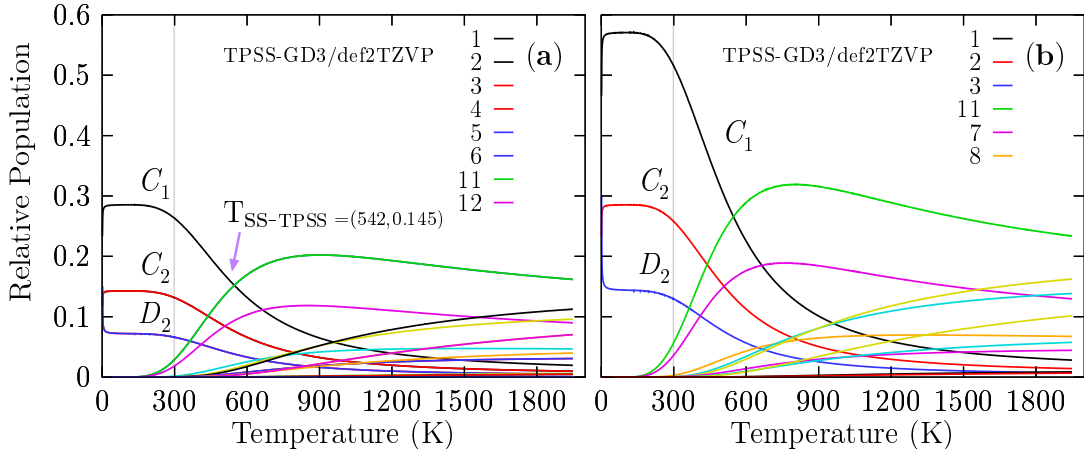


FIG. 9: Probability occurrence of each isomers computed employing TPSS¹⁵⁵ functional with the def2TZVP basis set, taking into account version three of Grimme’s dispersion¹³⁶ as it is implemented in Gaussian code.¹²⁶ The relative energies between two isomers vary considerably with the functional use. This will affect the temperature-dependent Boltzmann factors computed for each isomer and, therefore, the relative population change, as shown in Figure. Employing TPSS functional. The T_{SS} point is located at 542 K on a temperature scale compared with the T_{SS} point located at 739 K when we employ the PBE0 functional.

For temperatures ranging from 20 to 542 K, the chiral structure, depicted in Figure 1(a), strongly dominates as a global minimum. At 542 K, a type-helix chiral structure coexists, depicted Figure 1(k), with the chiral putative global minimum at cold temperatures. For temperatures ranging from 543 to 1600 K, the chiral structure’s type-helix chiral structure dominates as the putative global minimum. A large difference between the TSS point computed with TPSS functional¹⁵⁵ and that computed with PBE0 functional¹²⁸. Thus, it is important to choose the DFT functionals and basis that better describe the system to calculate the relative population and any Boltzmann weighted property.

Appendix B: Be-Be and B-B bond length evolution for enantiomers

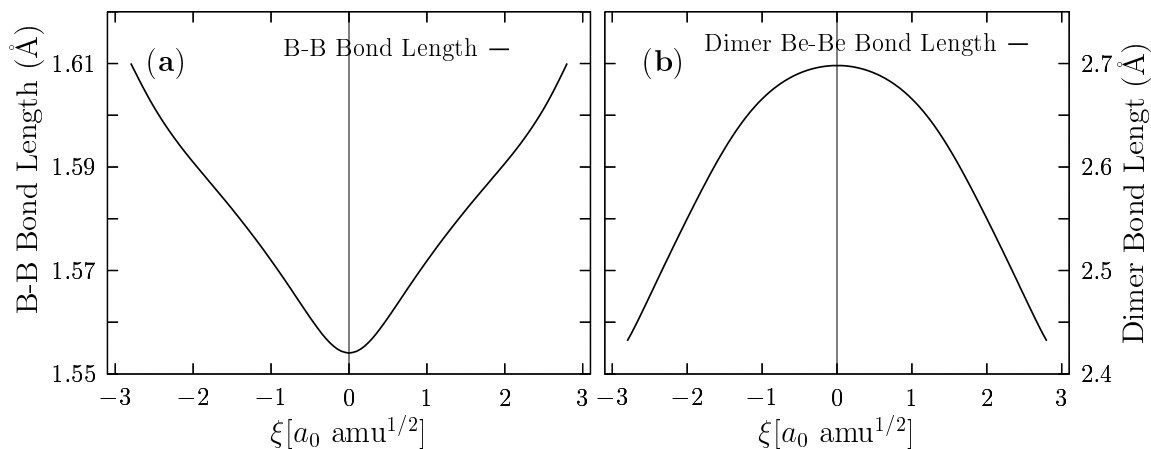


FIG. 10: Panel (a) shows the bond length evolution of the Be-Be dimer that is capping one side of the distorted ring boron along the IRC of the chiral Be_4B_8 cluster. Panel (b) shows the evolution distance between the two dimers that are capping the distorted ring boron along the IRC of the chiral Be_4B_8 cluster. In panel (a), the minimum Be-Be bond length is located at TS state with value of 1.9416 Å, and the maximum value is 1.9862 Å that correspond to one of the putative global minimum. The largest rate of decreasing/increasing bond length of Be-Be dimer is happening when the reaction start/end, before or after of the point of maximum force.

Appendix C: Energy of enantiomerization

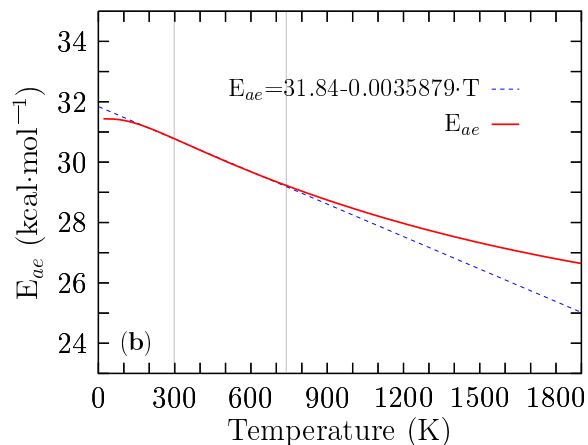


FIG. 11: We show a perfect line depicted in the blue dashed line overlapping to energy barrier for enantiomers in the temperature range 200 to 740 K.

Appendix D: IR Harmonic vs Anharmonic spectra

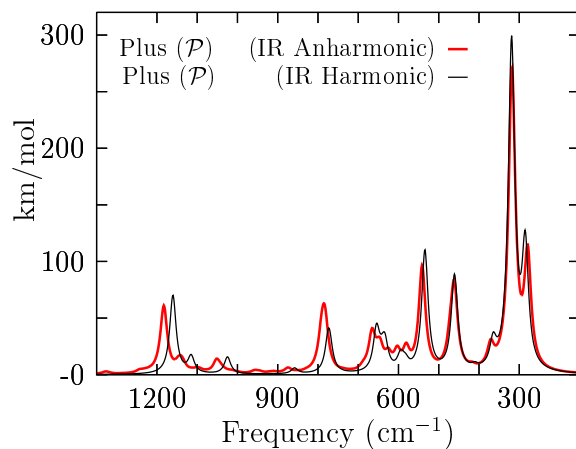


FIG. 12: We show a comparison between IR Harmonic vs IR Anharmonic spectra. IR-Harmonic spectrum was scaled by 0.96 to overlap the IR Anharmonic spectrum. The full width at half maximum (FWHM) employed is 20cm^{-1}

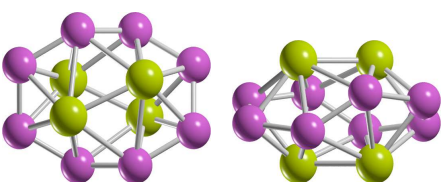
Appendix E: XYZ atomic coordiantes

12

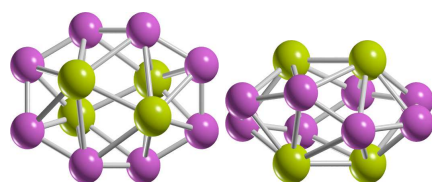
```
0.000000000      cluster_0002.out
Be -0.905655000000 -0.409167000000 -1.143981000000
Be  0.906419000000 -0.409960000000  1.144242000000
Be -0.905173000000  0.408402000000  1.143806000000
Be  0.905131000000  0.410037000000 -1.143131000000
B  -0.682576000000 -1.497315000000  0.425977000000
B  -0.684257000000  1.498360000000 -0.425282000000
B   0.684218000000 -1.498348000000 -0.426351000000
B   0.682942000000  1.498649000000  0.425686000000
B  -2.072794000000  0.728212000000 -0.251748000000
B   2.072272000000 -0.728536000000 -0.252462000000
B   2.071532000000  0.729531000000  0.251631000000
B  -2.071915000000 -0.730003000000  0.251800000000
```

12

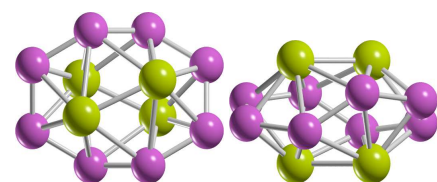
```
0.000000000      cluster_0001.out
Be -0.905655000000 -0.409167000000  1.143981000000
Be  0.906419000000 -0.409960000000 -1.144242000000
Be -0.905173000000  0.408402000000 -1.143806000000
Be  0.905131000000  0.410037000000  1.143131000000
B  -0.682576000000 -1.497315000000 -0.425977000000
B  -0.684257000000  1.498360000000  0.425282000000
B   0.684218000000 -1.498348000000  0.426351000000
B   0.682942000000  1.498649000000 -0.425686000000
B  -2.072794000000  0.728212000000  0.251748000000
B   2.072272000000 -0.728536000000  0.252462000000
B   2.071532000000  0.729531000000 -0.251631000000
B  -2.071915000000 -0.730003000000 -0.251800000000
```



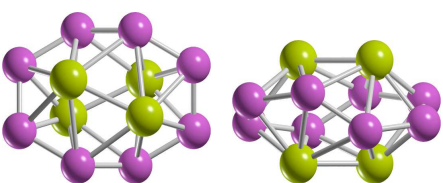
a(0.0)[**28.0%**](C_1)



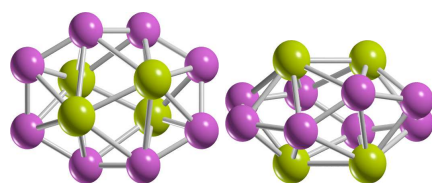
b(0.0)[**28.0%**](C_1)



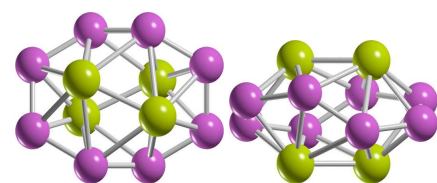
c(0.41)[**14.0%**](C_2)



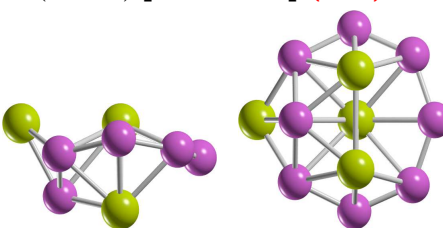
d(0.41)[**14.0%**](C_2)



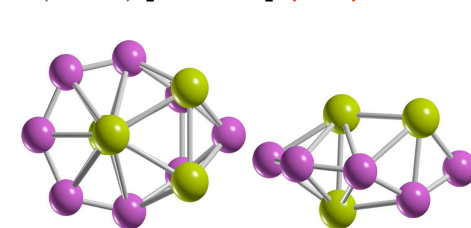
e(0.81)[**7.0%**](D_2)



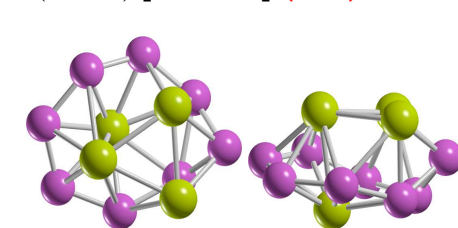
f(0.81)[**7.0%**](D_2)



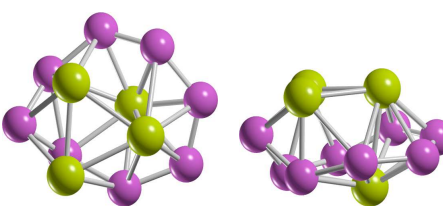
g(1.79)[**1.35%**](C_s)



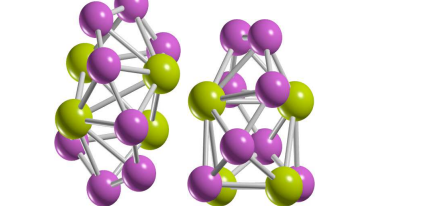
h(2.40)[**0.48%**](C_1)



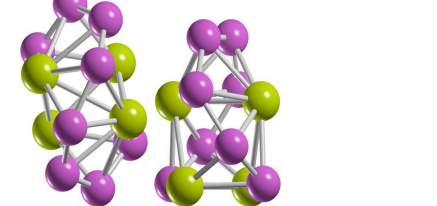
i(4.45)[**0.01%**](C_1)



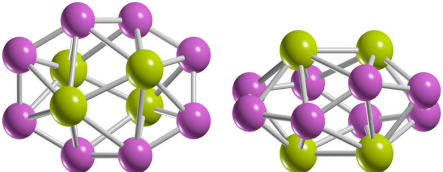
j(4.45)[**0.0%**](C_1)



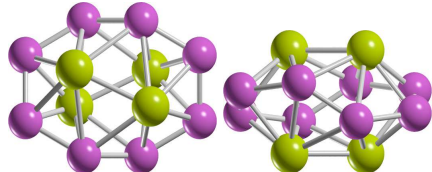
k(4.70)[**0.0%**](C_2)



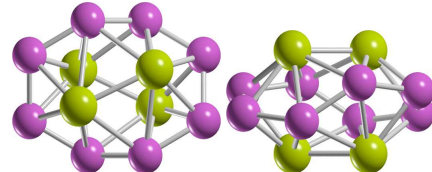
l(4.70)[**0.0%**](C_2)



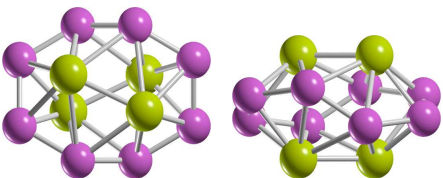
a(0.0)[**28.0%**](C_1)



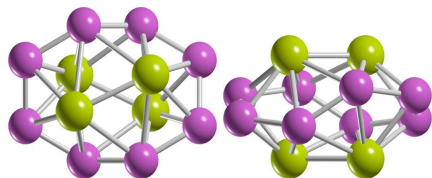
b(0.0)[**28.0%**](C_1)



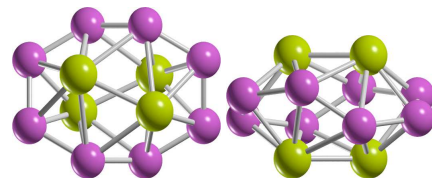
c(0.41)[**14.0%**](C_2)



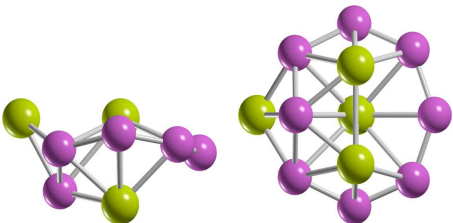
d(0.41)[**14.0%**](C_2)



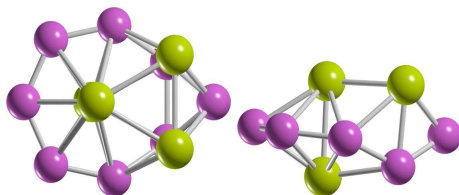
e(0.81)[**7.0%**](D_2)



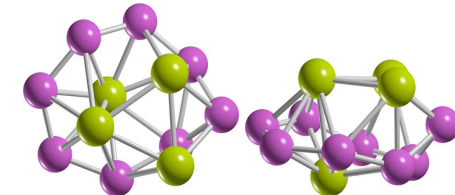
f(0.81)[**7.0%**](D_2)



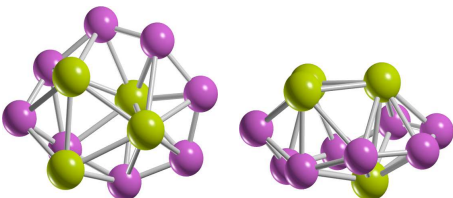
g(1.79)[**1.35%**](C_s)



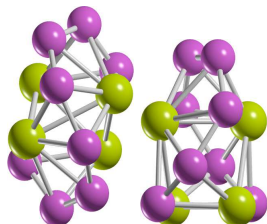
h(2.40)[**0.48%**](C_1)



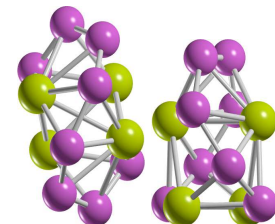
i(4.45)[**0.01%**](C_1)



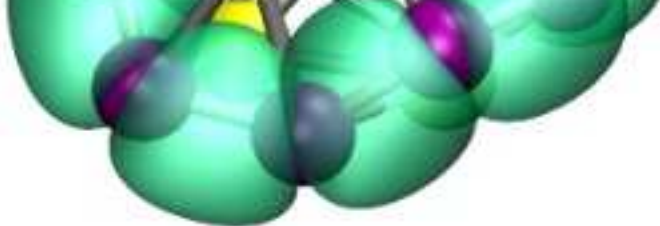
j(4.45)[**0.0%**](C_1)



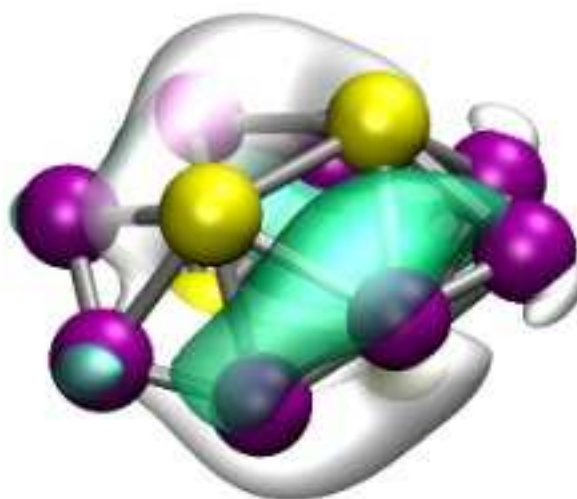
k(4.70)[**0.0%**](C_2)



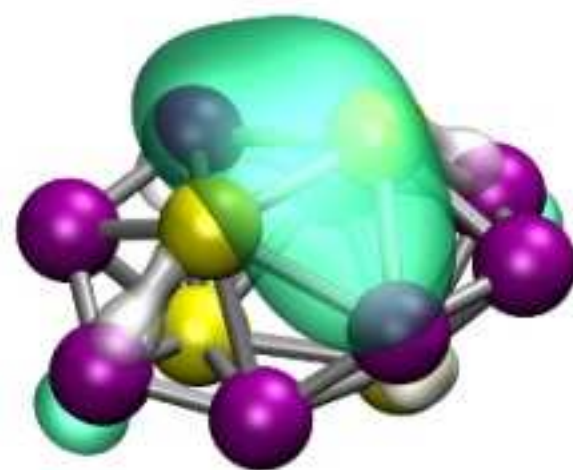
l(4.70)[**0.0%**](C_2)



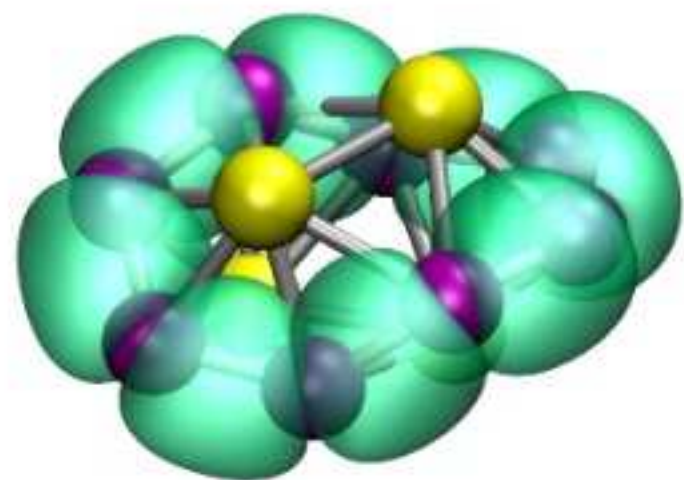
8x2c-2e B-B σ -bonds
ON = 1.92-1.94 |e|



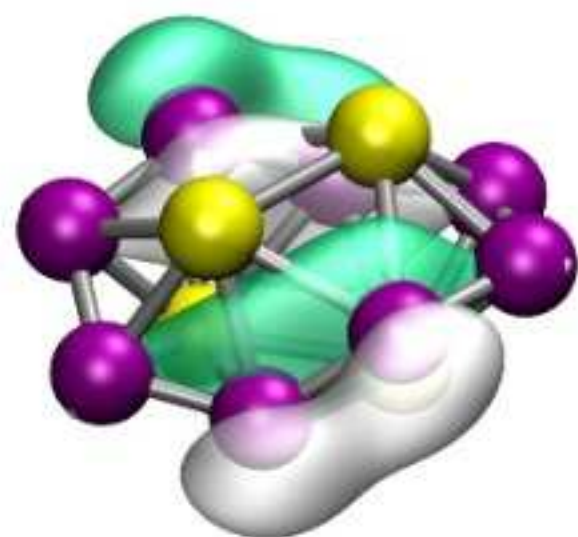
8c-2e n-bond
ON = 1.92 |e|



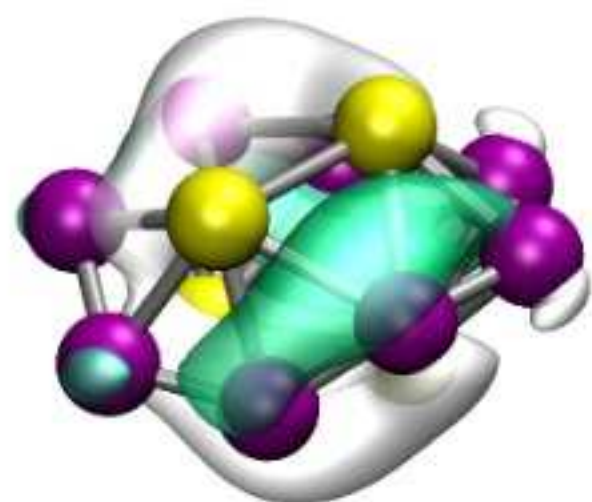
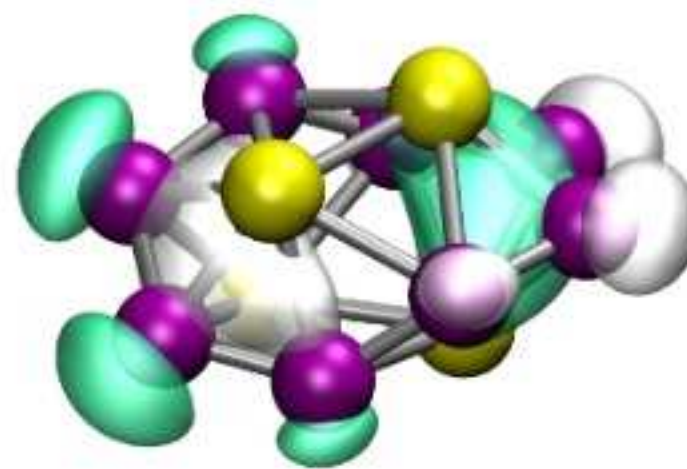
2x6c-2e
ON =



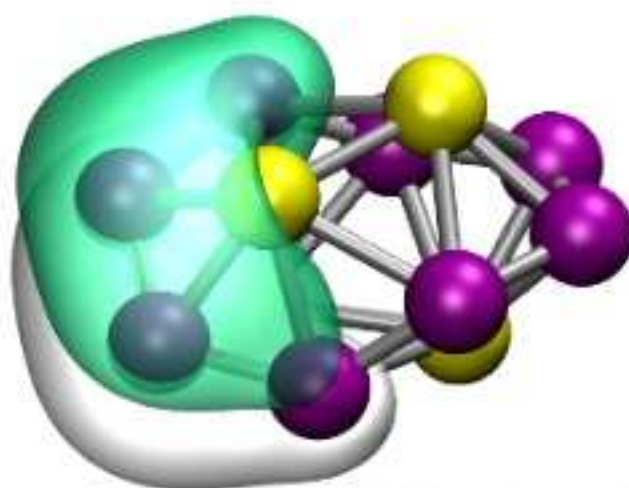
8x2c-2e B-B σ -bonds
ON = 1.92-1.94 |e|



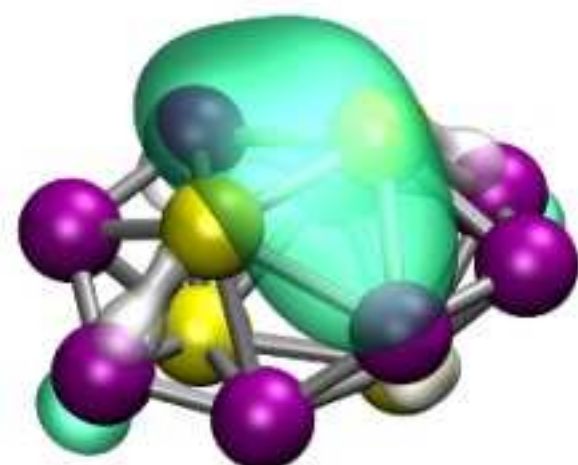
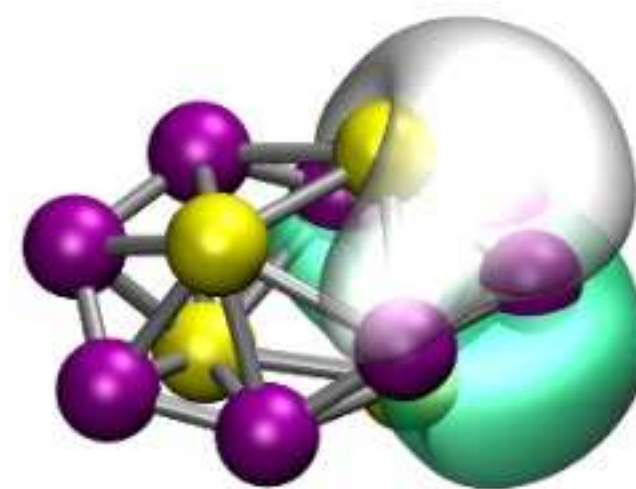
3x8c-2e σ -bonds
ON = 1.95-1.99 |e|



8c-2e π -bond
ON = 1.92 |e|



2x6c-2e π -bonds
ON = 1.99 |e|



2x6c-2e σ -bonds
ON = 1.91 |e|

